Improved Extratropical North Atlantic Atmosphere–Ocean Variability with Increasing Ocean Model Resolution

CASEY R. PATRIZIO,[a] PANOS J. ATHANASIADIS,[a] CLAUDE FRANKIGNOUL,[b,c] DOROTEACIRO IOVINO,[a] SIMONA MASINA,[a] LUCA FAMOOSS PAOLINI,[a,d] AND SILVIO GUALDI[a]

[a] *Centro Euro-Mediterraneo sui Cambiamenti Climatici (CMCC), Bologna, Italy*
[b] *Sorbonne University, Paris, France*
[c] *Woods Hole Oceanographic Institution, Woods Hole, Massachusetts*
[d] *Department of Physics and Astronomy, University of Bologna, Bologna, Italy*

(Manuscript received 20 April 2023, in final form 14 August 2023, accepted 18 September 2023)

ABSTRACT: North Atlantic atmosphere–ocean variability is assessed in climate model simulations from HighResMIP that have low resolution (LR) or high resolution (HR) in their atmosphere and ocean model components. It is found that some of the LR simulations overestimate the low-frequency variability of subpolar sea surface temperature (SST) anomalies and underestimate its correlation with the NAO compared to ERA5. These deficiencies are significantly reduced in the HR simulations, and it is shown that the improvements are related to a reduction of intrinsic (non-NAO-driven) variability of the subpolar ocean circulation. To understand the cause of the overestimated intrinsic subpolar ocean variability in the LR simulations, a link is demonstrated between the amplitude of the subpolar ocean variability and the mean state of the Labrador–Irminger Seas. Supporting previous studies, the Labrador–Irminger Seas tend to be colder and fresher in the LR simulations compared to the HR simulations and oceanic observations from EN4. This promotes upper-ocean density anomalies in this region to be more salinity-controlled in the LR simulations versus more temperature-controlled in the HR simulations and EN4 observations. It is argued that this causes the excessive subpolar ocean variability in the LR simulations by favoring a positive feedback between subpolar upper-ocean salinity and Atlantic meridional overturning circulation (AMOC) anomalies, rather than a negative feedback between subpolar SST and AMOC anomalies as in the HR simulations. The findings overall suggest that the subpolar ocean mean state impacts the variability of the ocean circulation and SSTs, including their relationship with the atmospheric circulation, in the extratropical North Atlantic.

KEYWORDS: North Atlantic Ocean; Atmosphere-ocean interaction; Ocean circulation; Model comparison; Model errors; Decadal variability

1. Introduction

Heat and momentum exchanges between the atmosphere and ocean are critical for establishing the mean climate but are also related to climate variability across a range of spatiotemporal scales in both media. In the North Atlantic, such atmosphere–ocean variability is often associated with large-scale climate anomalies on subseasonal to multidecadal time scales that can impact the climates of surrounding regions (e.g., Knight et al. 2006; Zhang and Delworth 2006). Global climate models can be used as tools to help understand the causes of such climate variability and to potentially predict the associated climate anomalies (e.g., Scaife et al. 2014; Årthun et al. 2017; Simpson et al. 2019; Athanasiadis et al. 2020). In practice, however, climate models generally suffer from biases in both their atmospheric and oceanic model components that degrade the realism of the simulated variability in the North Atlantic region and in turn the potential for prediction (e.g., Lee et al. 2018; Smith et al. 2020; Roberts et al. 2021). A deeper understanding of the mechanisms of North Atlantic atmosphere–ocean variability and its representation in climate models is thus a key step toward improving climate simulations and predictions.

In this study, we focus on the large-scale atmosphere–ocean variability in the extratropical North Atlantic, which remains incompletely understood. This variability has been linked to teleconnections from the tropical Pacific (e.g., Lau and Nath 2001), but to a large extent it can be explained by atmosphere–ocean interactions within the basin (e.g., Marshall et al. 2001a). Early studies hypothesized that sea surface temperature (SST) variability is primarily forced by surface heat fluxes associated with the atmospheric circulation (e.g., Frankignoul and Hasselmann 1977), but in more recent studies the ocean circulation has been hypothesized to play a more active role. In particular, it has been shown that SST anomalies can arise from variability of the Gulf Stream (e.g., Dong and Kelly 2004), the subtropical and subpolar gyres (e.g., Häkkinen et al. 2011; Piecuch et al. 2017), and the Atlantic meridional

Denotes content that is immediately available upon publication as open access.

Supplemental information related to this paper is available at the Journals Online website: https://doi.org/10.1175/JCLI-D-23-0230.s1.

Corresponding author: Casey Patrizio, casey.patrizio@cmcc.it

Publisher's Note: This article was revised on 28 November 2023 to correct the sizing of Fig. 10.

DOI: 10.1175/JCLI-D-23-0230.1

© 2023 American Meteorological Society. This published article is licensed under the terms of the default AMS reuse license. For information regarding reuse of this content and general copyright information, consult the AMS Copyright Policy (www.ametsoc.org/PUBSReuseLicenses).

Brought to you by UNIV BOLOGNA-CAMPUS RAVENNA | Unauthenticated | Downloaded 02/14/24 03:05 PM UTC

overturning circulation (AMOC) (e.g., Buckley and Marshall 2016; Zhang et al. 2019), each of which has been linked to oceanic circulation responses to surface wind stress and/or buoyancy fluxes associated with atmospheric circulation variability (e.g., Eden and Willebrand 2001; Frankignoul et al. 2001; Kwon and Frankignoul 2012; Barrier et al. 2014; Yeager 2015; Delworth et al. 2017). Evidence has also emerged that North Atlantic SST variability may itself influence the atmospheric circulation (e.g., Gastineau and Frankignoul 2015; Wills et al. 2016; Ruggieri et al. 2021; Kwon et al. 2020; Famooss Paolini et al. 2022) and hence may reflect two-way interactions between the atmosphere and ocean. For example, studies have hypothesized that a positive feedback between the NAO and SST anomalies can enhance the low-frequency climate variability in the North Atlantic region (Czaja and Frankignoul 2002; Czaja et al. 2003; Ferreira and Frankignoul 2005) and that dynamical interactions between the atmospheric and oceanic circulations may promote low-frequency atmosphere–ocean oscillations (e.g., Bellucci et al. 2008; Sun et al. 2015; Martin et al. 2019; Wills et al. 2019; Årthun et al. 2021).

Many studies have used climate models to provide insights about the possible mechanisms of extratropical North Atlantic atmosphere–ocean variability, but these models generally suffer from biases in the representation of the variability and mean state of the atmosphere and ocean in the North Atlantic region. Regarding the variability, there has been reported evidence of overestimated low-frequency variance in extratropical SSTs in coarse-resolution simulations (Ba et al. 2014) and multimodel hindcasts (Danabasoglu et al. 2016), while other studies showed that the amplitudes of Atlantic multidecadal variability (AMV) simulated by CMIP5 models were generally underestimated (e.g., Cheung et al. 2017; Murphy et al. 2017; Yan et al. 2018). Likewise, model deficiencies have been demonstrated for the variability of the extratropical atmospheric circulation, including underestimated decadal variability of the extratropical jet and the NAO (e.g., Simpson et al. 2018; Kim et al. 2018; O'Reilly et al. 2021). Regarding the mean state, major model biases in the SST climatology have been linked to misrepresentations of the Gulf Stream and its extension (e.g., Danabasoglu 2008; Danabasoglu et al. 2013; Chassignet et al. 2020) and to aspects of the extratropical atmospheric circulation, such as the position and strength of the eddy-driven jet and the associated blocking frequency (Scaife et al. 2011; Keeley et al. 2012; Lee et al. 2018; Athanasiadis et al. 2022). There is also evidence that biases in the mean state and variability of the North Atlantic are related. For example, Danabasoglu et al. (2016) suggested that model biases in the patterns and magnitudes of extratropical SST anomalies were partly due to biases in mean SSTs resulting from an incorrect representation of the North Atlantic Current. Furthermore, Menary et al. (2015a) found that CMIP5 biases in the mean SST and sea surface salinity in the Labrador Sea region were related to biases in the salinity control versus temperature control of upper-ocean density anomalies in this region.

One possible source of such model biases is insufficient grid resolution. With a resolution that is too coarse, small-scale processes like mesoscale ocean eddies and atmospheric convection must be parameterized. Ocean model resolution is also important for resolving bottom topography, which can influence the orientation and strength of ocean currents. For example, increased ocean model resolution generally improves the representation of the Gulf Stream, leading to improvements in SSTs and air–sea heat fluxes around this region, particularly in the Gulf Stream Extension area (e.g., Bryan et al. 2007; Small et al. 2019; Bellucci et al. 2021; Athanasiadis et al. 2022). Increased ocean model resolution tends to be associated with a stronger and more realistic mean subpolar gyre and AMOC (e.g., Hewitt et al. 2020; Hirschi et al. 2020; Roberts et al. 2020; Meccia et al. 2021), which enhances poleward heat transport and improves simulation of the mean SSTs, sea surface salinity, and sea ice cover in the high-latitude North Atlantic (Hewitt et al. 2016; Grist et al. 2018; Menary et al. 2018; Docquier et al. 2019). Increased model resolution in both the atmospheric and oceanic components has been linked to improvements in some aspects of the atmospheric circulation over the North Atlantic, such as the atmospheric response to Gulf Stream variability (e.g., Famooss Paolini et al. 2022) and atmospheric blocking over Europe and Greenland (e.g., Schiemann et al. 2020; Athanasiadis et al. 2022).

In this study, we investigated the impacts of increasing model resolution on the representation of North Atlantic atmosphere–ocean variability by analyzing multimodel output from HighResMIP simulations. Previous studies have used model output from HighResMIP to provide insights about the impacts of increased horizontal model resolution on the AMOC (Roberts et al. 2020; Jackson et al. 2020), the gyre circulations (Meccia et al. 2021), deep convection in the Labrador Sea (Koenigk et al. 2021), air–sea interactions over the Gulf Stream (Bellucci et al. 2021), the atmospheric response to Gulf Stream variability (Famooss Paolini et al. 2022), atmospheric blocking (Schiemann et al. 2020), Euro-Atlantic weather regimes (Fabiano et al. 2020), and relationships between the mean SSTs and the eddy-driven jet (Athanasiadis et al. 2022). However, model output from HighResMIP has not yet been used to examine the impacts of increased model resolution on the large-scale variability of North Atlantic SSTs, and the associated variability in the atmospheric and oceanic circulations. The purpose of this study is thus to provide more robust conclusions regarding the impacts of increasing model resolution on the representation of large-scale atmosphere–ocean variability in the North Atlantic compared to studies focusing on single models.

2. Methods

a. *Model output and observation-based data*

The multimodel output analyzed in this study follows the HighResMIP protocol (Haarsma et al. 2016), which offers a unified framework for investigating the impacts of model resolution on the simulated climate. The model output was primarily produced by the PRIMAVERA (Process-Based Climate Simulation: Advances in High Resolution Modelling and European Climate Risk Assessment) project, which includes output from CMCC-CM2 (Cherchi et al. 2019), CNRM-CM6 (Voldoire et al. 2019), EC-Earth3P (Haarsma et al. 2020), ECMWF-IFS (Roberts et al.

Brought to you by UNIV BOLOGNA-CAMPUS RAVENNA | Unauthenticated | Downloaded 02/14/24 03:05 PM UTC

TABLE 1. HighResMIP models analyzed in this study. Columns indicate the model name, the atmospheric grid spacing at 50°N, nominal oceanic grid spacing, the number of ensemble members for the historical and control runs, and the model resolution categorization (LR, MR, or HR) as defined in the text. The models in boldface indicate the models with multiple members in the historical runs.

No.	Model	Atmospheric grid (km)	Oceanic grid (km)	No. of members (hist-1950)	No. of members (control-1950)	Resolution
1	CMCC-CM2-HR4	64	25	1	1	MR
2	CMCC-CM2-VHR4	18	25	1	1	HR
3	CNRM-CM6-1	142	100	1	1	LR
4	CNRM-CM6-1-HR	50	25	1	1	MR
5	**EC-Earth3P**	**71**	**100**	**3**	**3**	**LR**
6	**EC-Earth3P-HR**	**36**	**25**	**3**	**3**	**HR**
7	**ECMWF-IFS-LR**	**50**	**100**	**8**	**1**	**LR**
8	ECMWF-IFS-MR	50	25	–	1	MR
9	**ECMWF-IFS-HR**	**25**	**25**	**6**	**1**	**HR**
10	**HadGEM3-GC31-LL**	**135**	**100**	**8**	**1**	**LR**
11	HadGEM3-GC31-MM	60	25	–	1	MR
12	**HadGEM3-GC31-HM**	**25**	**25**	**6**	**1**	**HR**
13	MPI-ESM1-2-HR	67	40	1	1	LR
14	MPI-ESM1-2-XR	34	40	1	1	MR
15	CESM1-CAM5-SE-LR	60	100	1	1	LR
16	CESM1-CAM5-SE-HR	20	10	1	1	HR

2018), HadGEM3-GC31 (Roberts et al. 2019), MPI-ESM1-2 (Gutjahr et al. 2019), and AWI-CM-1.0 (Sein et al. 2017). However, AWI was not analyzed due to missing output. We also analyzed model output from CESM1-CAM5 (Meehl et al. 2019; Hurrell et al. 2020a,b), which was not part of PRIMAVERA. Note that nearly all climate models analyzed in this study use the same ocean model component, NEMO, except for the MPI model, which uses MPIOM1.63 and the CESM model, which uses POP2. Both historical (hist-1950) and control (control-1950) runs were analyzed for each model, which in some cases provide multiple realizations (ensemble members) with slightly varying initial conditions (Table 1). As documented in Haarsma et al. (2016), the historical simulations were integrated for 65 years with observed radiative forcings corresponding to the 1950–2014 period, whereas the control simulations were integrated for 100 years with constant radiative forcings corresponding to the year 1950.

As shown in Table 1, each model generally provides output for a lower-resolution and higher-resolution configuration. However, in CMCC-CM2 and MPI-ESM1-2 only the resolution of the atmospheric component was increased. In addition to their lower- and higher-resolution configurations, ECMWF-IFS and HadGEM-GC31 also provide a set of runs with low-resolution in the atmosphere model and high-resolution in the ocean model (affixed with "MR" and "MM" respectively in Table 1), which we analyzed in order to isolate the impact of increased ocean model resolution alone.

Since the exact atmospheric and oceanic model resolutions differ between models, we defined low-resolution (LR) models as those with atmospheric resolution $\geq$ 50 km at 50°N and a nominal oceanic resolution $>$ 25 km, and high-resolution (HR) models as those with atmospheric resolution $<$ 50 km at 50°N and a nominal oceanic resolution $\leq$ 25 km. The remaining models are defined as medium-resolution (MR) models, which have an LR atmosphere model and an HR ocean model, or vice versa. With these definitions, nearly all of the LR models have ~1° oceanic resolution and nearly all of the HR models have ~0.25° oceanic resolution, whereas the atmospheric resolution is more variable among models. Furthermore, four out of the seven models have both LR and HR configurations: ECMWF, EC-Earth, HadGEM and CESM. The remaining models (CNRM, CMCC, and MPI) have only MR and LR or MR and HR configurations. To account for the large internal variability inherent to the extratropics, we focused our analyses on models with multiple members in the LR and HR historical runs, namely ECMWF, EC-Earth, and HadGEM (the models in bold in Table 1). Hence, multimodel means for the LR and HR models were calculated from these three models, unless otherwise specified. A subset of analyses was performed for all models.

From the model output, we acquired monthly-averaged SST, surface heat fluxes (sum of sensible, latent, and radiative heat fluxes), sea level pressure (SLP), meridional ocean currents, mixed layer depth (MLD), and ocean salinities and temperatures averaged over the upper 500 m. Model output was also compared to the ERA5 atmospheric dataset (Hersbach et al. 2020) and to the optimally interpolated EN4 oceanic dataset, version 4.2.2 (Good et al. 2013). Monthly-averaged SST, surface heat fluxes, and SLP were acquired from ERA5 between 1959 and 2021 and upper-ocean salinities and temperatures were acquired from EN4 over the same period. We did not compare the simulated ocean currents with observational estimates because of limited temporal and spatial coverage of observations for ocean currents over the historical period as well as discrepancies among ocean reanalyses in the variability of the ocean circulation over the last few decades (Karspeck et al. 2017; Jackson et al. 2019).

b. *Calculation of anomalies*

To analyze the climate variability, monthly anomalies were first calculated by subtracting the climatological monthly

Brought to you by UNIV BOLOGNA-CAMPUS RAVENNA | Unauthenticated | Downloaded 02/14/24 03:05 PM UTC

mean from each field. For the historical output, ERA5, and EN4 data, we removed the component of the fields at each grid point that is linearly related to the global-mean SST in order to help reduce the impact of external radiative forcings that have been linked to North Atlantic SST variability (e.g., Bellomo et al. 2018; Murphy et al. 2021). Although there are more effective methods to do so, removing the linear regression onto the global-mean SST is generally preferable to removing the linear trend (Frankignoul et al. 2017; Deser and Phillips 2021). For the control runs, the linear trend was removed in order to reduce climate drift (Haarsma et al. 2016). In general, either winter-mean [December–March (DJFM)] or annual-mean anomalies were analyzed to investigate the interannual variability, and a 7-yr low-pass Butterworth filter was applied to isolate the low-frequency (decadal to multidecadal) variability. The main results are rather insensitive to whether winter or annual-mean anomalies are used.

c. Calculation of horizontal upper-ocean streamfunction and overturning streamfunction

Different components of the ocean circulation were quantified by calculating a horizontal upper-ocean streamfunction (Ψ_{500}) and an overturning streamfunction (Ψ_V) from the meridional currents in the North Atlantic basin adopting methods from Marzocchi et al. (2015). For Ψ_{500}, the meridional currents (v) were vertically integrated over the upper 500 m of the ocean, and then zonally integrated from each point to the eastern boundary; that is,

$$\Psi_{500}(x, y) = -\int_{-500}^{0}\int_{x}^{x_e} v(x', y, z)dx'dz, \tag{1}$$

where x_e denotes the eastern boundary of the North Atlantic basin at latitude y and depth z.

For Ψ_V, the meridional currents were zonally integrated and then depth-integrated as follows:

$$\Psi_V(y, z) = \int_{z}^{0}\int_{x_w}^{x_e} v(x, y, z')dxdz', \tag{2}$$

where x_w corresponds to the western boundary in the North Atlantic basin at latitude y and depth z'. Prior to calculating the streamfunctions, the ocean currents were spatially smoothed with a 2D Gaussian kernel filter applied to a $5^\circ \times 5^\circ$ box with a standard deviation equal to 2. The purpose of the spatial smoothing is to remove the smaller-scale variability of ocean currents and hence target the larger-scale variability that we are interested in.

d. Indices of variability

The leading principal components (PCs) of SST and Ψ_{500} anomalies in the North Atlantic were calculated by EOF analysis over 0°–70°N, 0°–90°W using fields that have been spatially weighted (e.g., North et al. 1982; Baldwin et al. 2009) and concatenated across all ensemble members. We also used a station-based NAO index (Hurrell 1995) calculated from the standardized difference in monthly SLP anomalies between Lisbon, Portugal, and Reykjavik, Iceland, but other metrics of the atmospheric circulation variability were also tested (e.g., PC1 of SLP).

For analyses focused on the subpolar region, a subpolar SST index was defined by taking the area-weighted average of the SST anomalies within 50°–65°N, 5°–60°W (yellow box in Fig. 1), while a subpolar horizontal upper-ocean streamfunction index was calculated by taking the area-weighted average of Ψ_{500} over a slightly broader region centered over the subpolar gyre (45°–65°N, 5°–60°W; yellow box in Fig. 4). As a measure of the variability of the upper branch of the overturning circulation in the extratropics, an AMOC index was calculated by averaging Ψ_V between 40° and 60°N and between 500–2000 m depth.

e. Statistical significance testing

The statistical significance of lead–lag correlations between low-pass filtered variables was tested following a parametric bootstrapping method from Danabasoglu et al. (2016), which assumes that the annual-averaged anomalies of the variables being considered (e.g., the AMOC and subpolar SST) can be modeled as red noise with variance and lag-1 autocorrelation estimated from the model time series. Then, for each given lag, we tested the null hypothesis that the two time series are independent and have zero correlation. In practice, the statistical significance of the multimodel mean cross-correlations between two low-pass filtered variables was tested in the following way: we constructed 5000 samples of two independent time series of length N from a first-order autoregressive process with variance and lag-1 autocorrelation estimated from the model time series (unfiltered) being considered, where N is the number of years in the model time series. Low-pass filtering was applied after constructing the samples and then the correlation coefficient was computed for each of the 5000 samples at each lag. This procedure was repeated for each of the model runs in the multimodel mean correlation, and the results were averaged. If the actual multimodel mean correlation was found to be above 99.5% or below 0.5% of the 5000 samples of multimodel mean correlations, the correlation was considered statistically significant at the 1% level. A similar approach was followed for ERA5, except the 5% significance level was used.

f. Salinity versus temperature control of density anomalies

The salinity control versus temperature control of upper-ocean density anomalies was assessed following the method from Menary et al. (2015a), which assumes a linear decomposition of the equation of state into salinity- and temperature-related variations. First, the upper-ocean density (ρ_{500}) was calculated with the equation of state from the 0–500 m depth-averaged salinity and temperature fields. Then, the component of the density that arises only from salinity variations ($\rho_{S,500}$) or only from temperature variations ($\rho_{T,500}$) was calculated by holding temperature or salinity constant, respectively, at its climatological-mean value in the equation of state. This linear decomposition of the nonlinear equation of state is valid because ocean salinity and temperature anomalies are relatively small so that $\rho'_{500} \approx \rho'_{S,500} + \rho'_{T,500}$, where the prime denotes an anomaly. Finally, the salinity- versus temperature-control of density anomalies ($\rho_{S\text{vs}T\text{control}}$) was defined as in Menary et al. (2015a) by regressing ρ_{500} onto $\rho_{S,500}$ anomalies (denoted as

Brought to you by UNIV BOLOGNA-CAMPUS RAVENNA | Unauthenticated | Downloaded 02/14/24 03:05 PM UTC

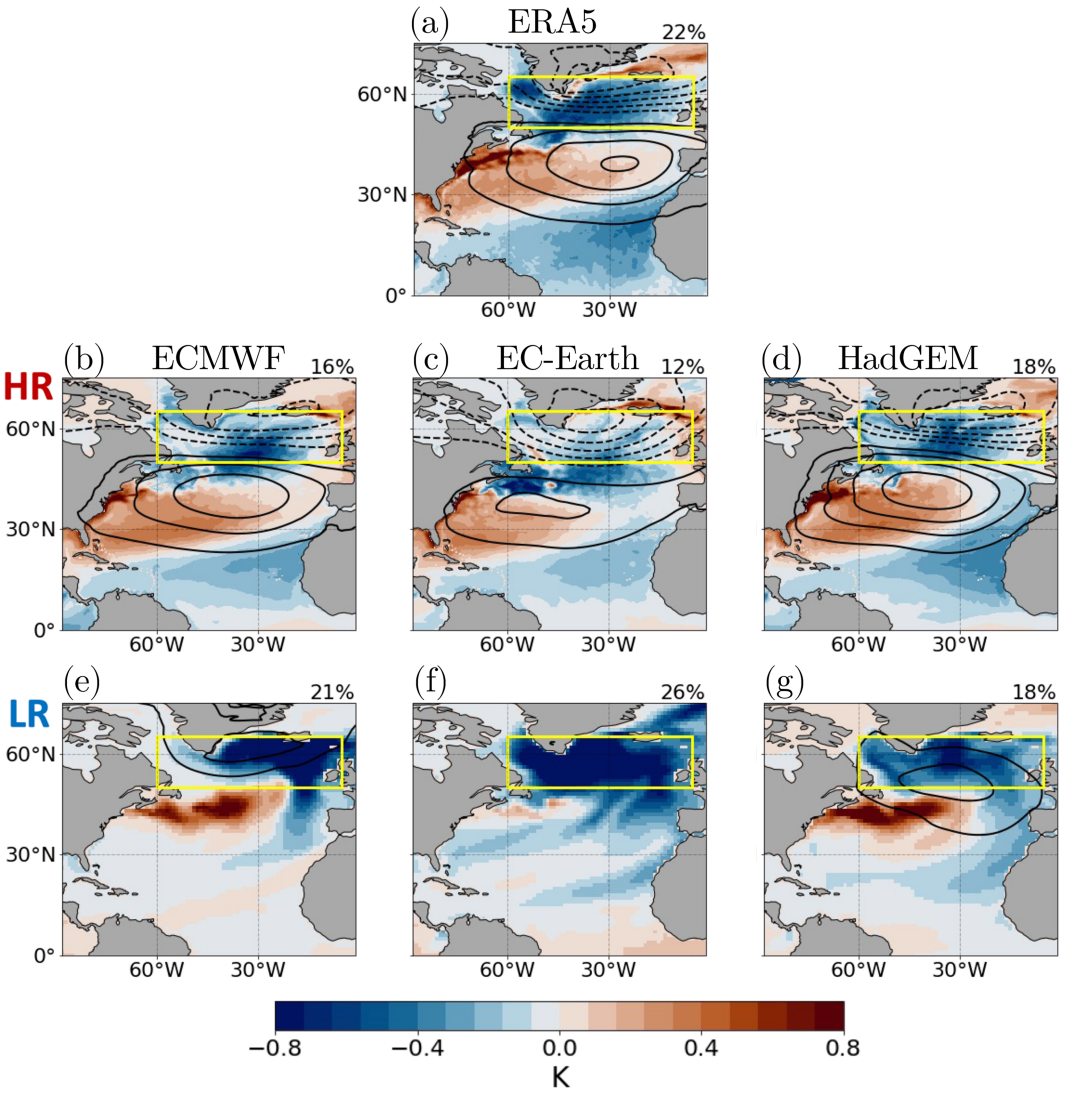

FIG. 1. Leading EOF of winter-mean (DJFM) SST anomalies (shading; K) calculated over the North Atlantic (0°–70°N, 0°–90°W), and SLP anomalies regressed onto the respective PCs (contours; 0.6 hPa interval and dashed contours are negative) for (a) ERA5, (b)–(d) the HR historical runs, and (e)–(g) the LR historical runs. The percentage of the total variance explained by each leading EOF is shown at the top right of each panel. The yellow box indicates the averaging region used to define the subpolar SST index.

r_{Scontrol}), regressing ρ_{500} onto $\rho_{T,500}$ anomalies (denoted as r_{Tcontrol}), and subtracting the difference between the resulting regression coefficients (i.e., $\rho_{\text{SvsTcontrol}} = r_{\text{Scontrol}} - r_{\text{Tcontrol}}$). Thus, positive values of $\rho_{\text{SvsTcontrol}}$ indicate that ρ_{500} variations are dominated by salinity anomalies, whereas negative values indicate that ρ_{500} variations are dominated by temperature anomalies.

3. Improved representation of large-scale SST variability in the HR simulations

a. *Leading EOF of SST and associated SLP anomalies*

We begin by discussing the representation of large-scale SST variability in the North Atlantic and its relationship with the atmospheric circulation in ERA5 and the historical runs for the LR and HR models. Figure 1a shows the leading EOF of North Atlantic SSTs and SLP regressed onto the leading PC of North Atlantic SSTs for ERA5 computed from winter-mean (DJFM) data, when atmosphere–ocean interactions are generally strongest. In ERA5 (Fig. 1a) and the HR models (Figs. 1b–d), the leading EOF of SSTs has a tripole-like structure and the associated SLP anomalies project significantly onto the NAO, which is consistent with prior observational studies (e.g., Cayan 1992; Visbeck et al. 2003; Deser et al. 2010). However, the LR models fail to capture the observed SST pattern and the associated NAO-like pattern of SLP anomalies (Figs. 1e–g). These models generally overestimate the SST variability in the subpolar North Atlantic region

Brought to you by UNIV BOLOGNA-CAMPUS RAVENNA | Unauthenticated | Downloaded 02/14/24 03:05 PM UTC

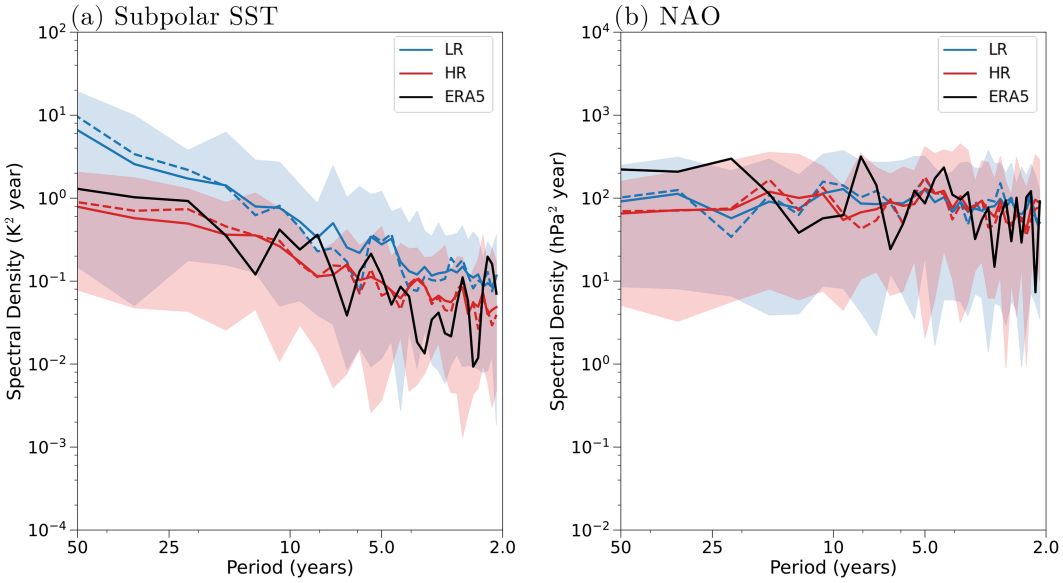

FIG. 2. (a) Power spectra of the subpolar SST index (K^2 yr) calculated with annual-mean anomalies from the historical runs (solid lines), control runs (dashed lines), and ERA5 (black line). Multimodel ensemble-mean spectra are calculated from the LR model runs (blue lines) and the HR model runs (red lines) and the associated spread across models runs indicated by transparent shading. (b) As in (a), except for the NAO index (hPa^2 yr) calculated with unstandardized DJFM-mean anomalies.

(45°–65°N) compared to ERA5, while associated SLP anomalies are weak and incoherent across models. Indeed, the correlation between the NAO and the subpolar SST index (SST anomalies averaged over the yellow box in Fig. 1) is not significantly different from zero for the multimodel mean of these three LR models, while the correlation is −0.50 for the multimodel mean of the HR models and −0.75 for ERA5.

The multimodel mean spectra of the subpolar SST index for these models indicate that the LR configurations (Fig. 2a; blue lines) exhibit greater power on decadal to multidecadal time scales compared to ERA5 and the respective HR configurations (Fig. 2a; red lines). Note that we did not detect statistically significant peaks (at the 5% significance level) on these time scales in the subpolar SST spectra for either the LR or HR multimodel mean or for ERA5, under the null hypothesis that the subpolar SST variability can be approximated as red noise. Consistent with the redder subpolar SST spectrum in the LR models, the multimodel ensemble mean lag-1 autocorrelation (r_1) of the subpolar SST index is larger in the historical LR model runs ($r_1 = 0.79$) than in the historical HR model runs ($r_1 = 0.55$) and ERA5 ($r_1 = 0.62$), with the control runs showing similar discrepancies ($r_1 = 0.88$ and $r_1 = 0.61$ for the LR and HR models, respectively). Hence, these results imply that the bias in the LR models is related to the low-frequency component of the variability and that this cannot be explained by variations in external radiative forcing. Indeed, the patterns of SLP and SST anomalies in Fig. 1 are qualitatively similar when applying a 7-yr low-pass filter to the fields prior to calculating the leading EOF of SST for both historical and control runs, except with somewhat underestimated amplitude in the HR models compared to ERA5 (Fig. S1 in the online supplemental material).

b. *Role of the NAO*

It is possible that the discrepancies in atmosphere–ocean variability between the LR and HR models could be partly explained by discrepancies in the power spectrum or variance of the NAO. For example, the stronger correlation between the NAO and SSTs in the HR models could be explained by a stronger NAO–SST feedback, which would act to enhance the persistence and low-frequency variance of the NAO in the HR models. However, this does not appear to be the case as the multimodel mean spectra of the unstandardized NAO index are approximately white and with similar amplitudes in the LR and HR model runs (Fig. 2b). The similar atmospheric forcing of SSTs in the LR and HR models is also reflected by a similar pattern of surface heat fluxes regressed onto the NAO index in both cases (not shown).

Interestingly, the NAO appears to have more low-frequency power in ERA5 than the LR and HR models, and consistently the NAO's persistence $r_1 = 0.27$ exceeds the maximum r_1 across all model runs. This is consistent with previous studies showing that climate models generally underestimate the low-frequency variance of the extratropical atmospheric circulation (e.g., Kim et al. 2018; Simpson et al. 2018; O'Reilly et al. 2021) and could be related to the misrepresentation of atmosphere–ocean feedbacks, eddy–mean flow interactions, and/or atmospheric teleconnections (e.g., Scaife and Smith 2018; Smith et al. 2019). However, this is seemingly inconsistent with results from Siqueira and Kirtman (2016) and Menary et al. (2018) showing that similar biases in the extratropical atmospheric circulation

Brought to you by UNIV BOLOGNA-CAMPUS RAVENNA | Unauthenticated | Downloaded 02/14/24 03:05 PM UTC

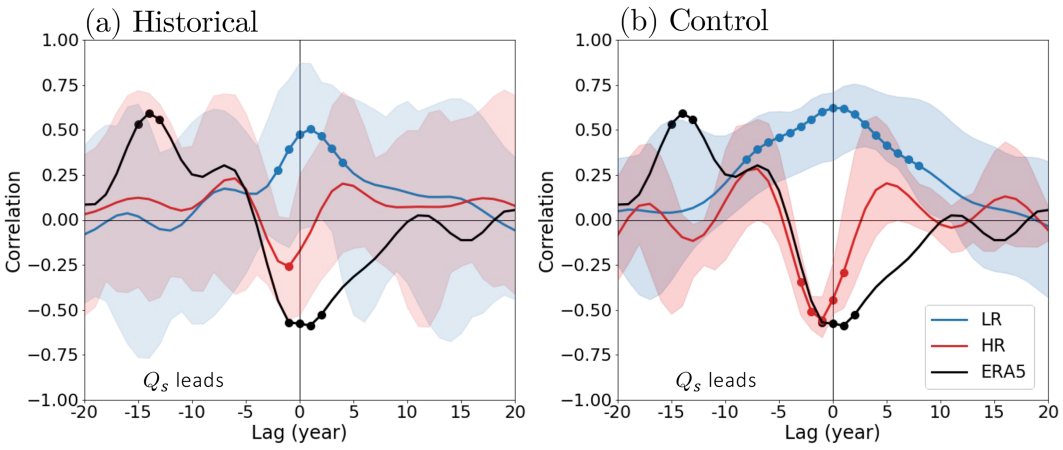

FIG. 3. Cross-correlation between the subpolar SST index and the surface heat fluxes (Q_s) averaged over the same region used to define the subpolar SST index for (a) the historical runs and (b) the control runs. The correlation for ERA5 is shown in each panel (black line). Negative lags indicate that the surface heat fluxes lead the subpolar SST index. Surface heat fluxes are defined as positive upward (i.e., heat loss by the ocean). Multimodel ensemble-mean correlations are calculated from the LR model runs (blue lines) and HR model runs (red lines) with the associated spread across the model runs indicated by transparent shading. Correlations that are found to be statistically significant (see section 2e) are indicated by round markers. All indices were calculated from 7-yr low-pass filtered DJFM-mean anomalies.

can be mitigated with higher model resolution. The apparent discrepancy with our findings could be due to the shorter 60–100-yr simulation period of HighResMIP compared to the multicentennial simulations of Menary et al. (2018), the coarser 0.25° oceanic resolution of the HighResMIP simulations compared to the higher 0.1°-resolution simulations of Siqueira and Kirtman (2016), and/or model differences in the representation of processes that may drive low-frequency variability of the NAO.

Overall, these results indicate that the discrepancies in atmosphere–ocean variability between the LR models and ERA5/HR models are not caused by discrepancies in the NAO, and hence are likely related to the ocean circulation. This is indirectly supported by multimodel mean cross-correlation between low-pass filtered surface heat fluxes and the subpolar SST index for the historical runs (Fig. 3a) and control runs (Fig. 3b). Notably, the negative correlation between surface heat fluxes and SSTs at around lags of 0–1 years in ERA5 and the HR models is consistent with subpolar SST anomalies being driven by the surface heat fluxes, but the positive correlation in the LR models is consistent with subpolar SST anomalies being damped by the surface heat fluxes. While not conclusive evidence, this suggests that ocean heat flux convergence anomalies may be driving the overestimated subpolar SST variability in the LR models.

Although the relationship between subpolar SSTs and surface heat fluxes is significantly improved in the HR models, Fig. 3 also indicates two notable discrepancies with ERA5. First, ERA5 shows a statistically significant positive correlation when the surface heat fluxes lead the SSTs by 15 years, which is not captured by the multimodel ensemble means of either the LR or HR models. Prior studies have interpreted such a relationship as the delayed response of the AMOC to the NAO (e.g., Delworth et al. 2017), suggesting that this ocean circulation response is not correctly represented even by HR models. However, some individual historical runs exhibit such positive correlations at large lags (see transparent shading in Fig. 3a) and hence the lagged correlation for ERA5 is within the spread of the models. Second, ERA5 also exhibits stronger negative correlations when the surface heat fluxes lag the SSTs. This is consistent with less persistent atmospheric forcing of subpolar SSTs in the models, possibly arising from underestimated atmosphere–ocean feedbacks as previously discussed.

4. Explaining the discrepancies between the LR and HR simulations: The role of the ocean circulation

In the following sections, we support the findings in the previous section by discussing the variability of the horizontal upper-ocean circulation and the AMOC. Unless otherwise indicated, results shown are calculated from 7-yr low-pass filtered annual-mean anomalies from the control runs, which better resolve the low-frequency component of the variability and generally show clearer discrepancies between the LR and HR models than the historical runs (e.g., see Figs. 3a,b).

a. Horizontal upper-ocean circulation

Figure 4 shows the leading EOF of low-pass filtered upper-ocean streamfunction anomalies, Ψ_{500} (defined in section 2c). The dominant pattern of low-frequency variability in Ψ_{500} clearly differs between the LR and HR models. On the one hand, the LR models generally exhibit the largest amplitude Ψ_{500} variability around the subpolar gyre (dashed lines) and hence represent changes in the strength and position of the subpolar gyre. On the other hand, the HR models generally exhibit the largest Ψ_{500} amplitude in a narrower midlatitude

Brought to you by UNIV BOLOGNA-CAMPUS RAVENNA | Unauthenticated | Downloaded 02/14/24 03:05 PM UTC

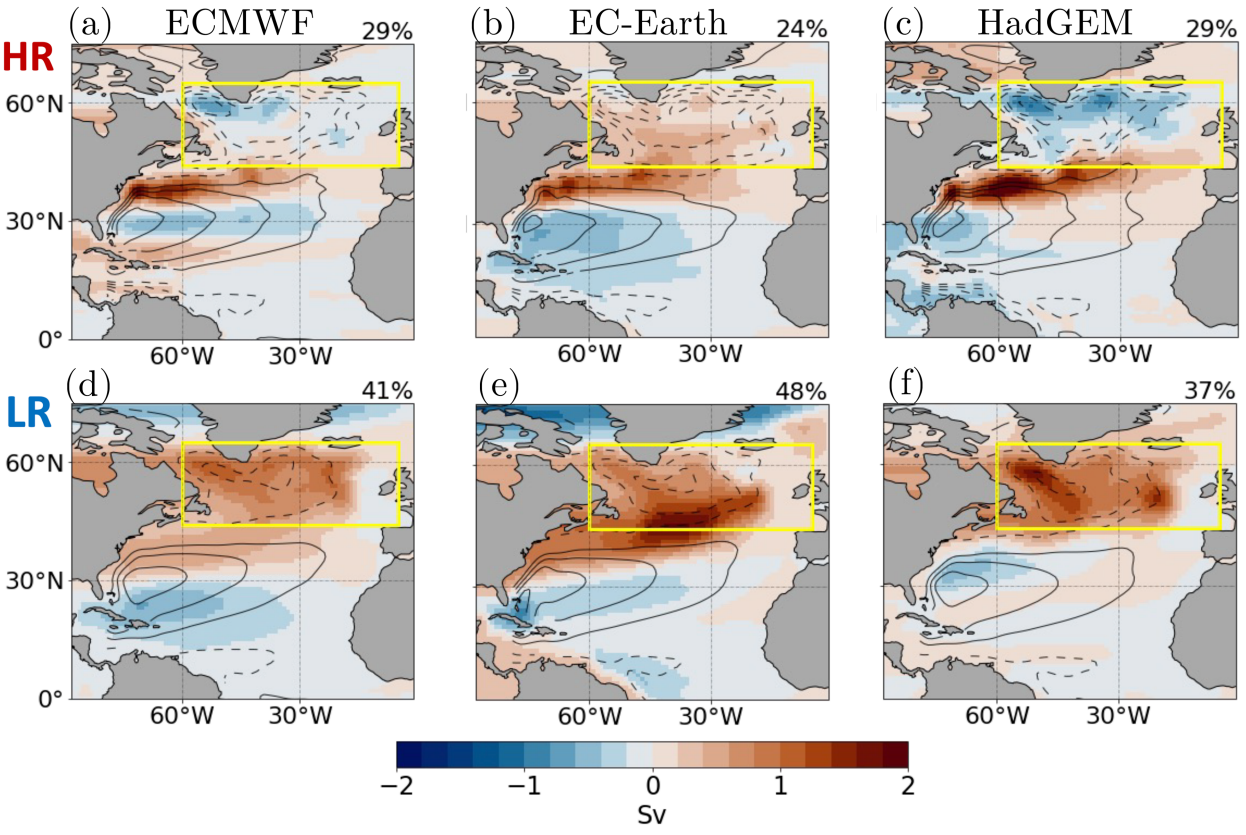

FIG. 4. The leading EOF of low-pass filtered Ψ_{500} anomalies [shading; Sv (1 Sv $\equiv 10^6$ m^3 s^{-1})] calculated over the North Atlantic (0°–70°N, 0°–90°W) for the (a)–(c) HR control runs and (d)–(f) LR control runs. The climatological mean Ψ_{500} is indicated by contours (5 Sv interval). The percentage of the total variance explained by the leading EOF is shown at the top right of each panel. The yellow box indicates the region used to define the subpolar Ψ_{500} index.

region between the subpolar and subtropical gyres. We interpret the latter as variability of the Gulf Stream (e.g., meridional shifts) as opposed to variability of the intergyre gyre, which is associated with barotropic (i.e., depth-integrated) circulation anomalies that more broadly traverse the boundary between the subpolar and subtropical gyres (e.g., Marshall et al. 2001b; Barrier et al. 2014; Meccia et al. 2021).

The results suggest that the upper-ocean subpolar gyre has greater low-frequency variability in the LR models than in the HR models, which could drive the bias in subpolar SSTs in the LR models. Indeed, Fig. 5e indicates that the standard deviations of the low-pass filtered subpolar SST and Ψ_{500} indices are positively correlated across all model runs ($r = 0.74$) with LR model runs (circle markers) generally having larger variances in both indices compared to HR model runs (diamond markers). This is reflected by averages across the LR and HR model runs (solid black markers), which also clearly indicate that the LR model runs overestimate the low-frequency variance of the subpolar SST index compared to ERA5 (vertical black line) while the HR model runs are closer to ERA5. The main exceptions are the LR runs of CNRM, MPI, and CESM, which provide only one member but exhibit more realistic subpolar SST variance like the HR runs. Possible explanations for these model differences are discussed in later sections. It is also noted that the LR model runs exhibit more spread and a stronger correlation between the standard deviations of the SST and Ψ_{500} indices ($r = 0.59$) compared to the HR models ($r = 0.36$). This could be because the surface heat fluxes likely play a relatively more important role than ocean circulation in driving subpolar SST anomalies in the HR models (Figs. 3a,b).

The greater low-frequency variability of the subpolar ocean in the LR models is also reflected by the autocorrelations for low-pass filtered subpolar SST and Ψ_{500} indices and the respective leading PCs (Figs. 5a–d). Clearly, these indices are more persistent in the LR models compared to the HR models (and ERA5 in the case of the SST indices). In general, the results shown in Fig. 5 suggest that understanding the causes of the greater persistence/low-frequency variance of the ocean circulation in the LR models is key to understanding the overestimated low-frequency variability in subpolar SSTs in these models.

Since variability of the subpolar gyre and the Gulf Stream (represented by the leading EOF of Ψ_{500} in the LR and HR models, respectively) has been linked to delayed ocean responses to NAO-related wind stress and buoyancy fluxes (e.g., Joyce et al. 2000; Curry and McCartney 2001; Eden and Willebrand 2001; Frankignoul et al. 2001; Lohmann

Brought to you by UNIV BOLOGNA-CAMPUS RAVENNA | Unauthenticated | Downloaded 02/14/24 03:05 PM UTC

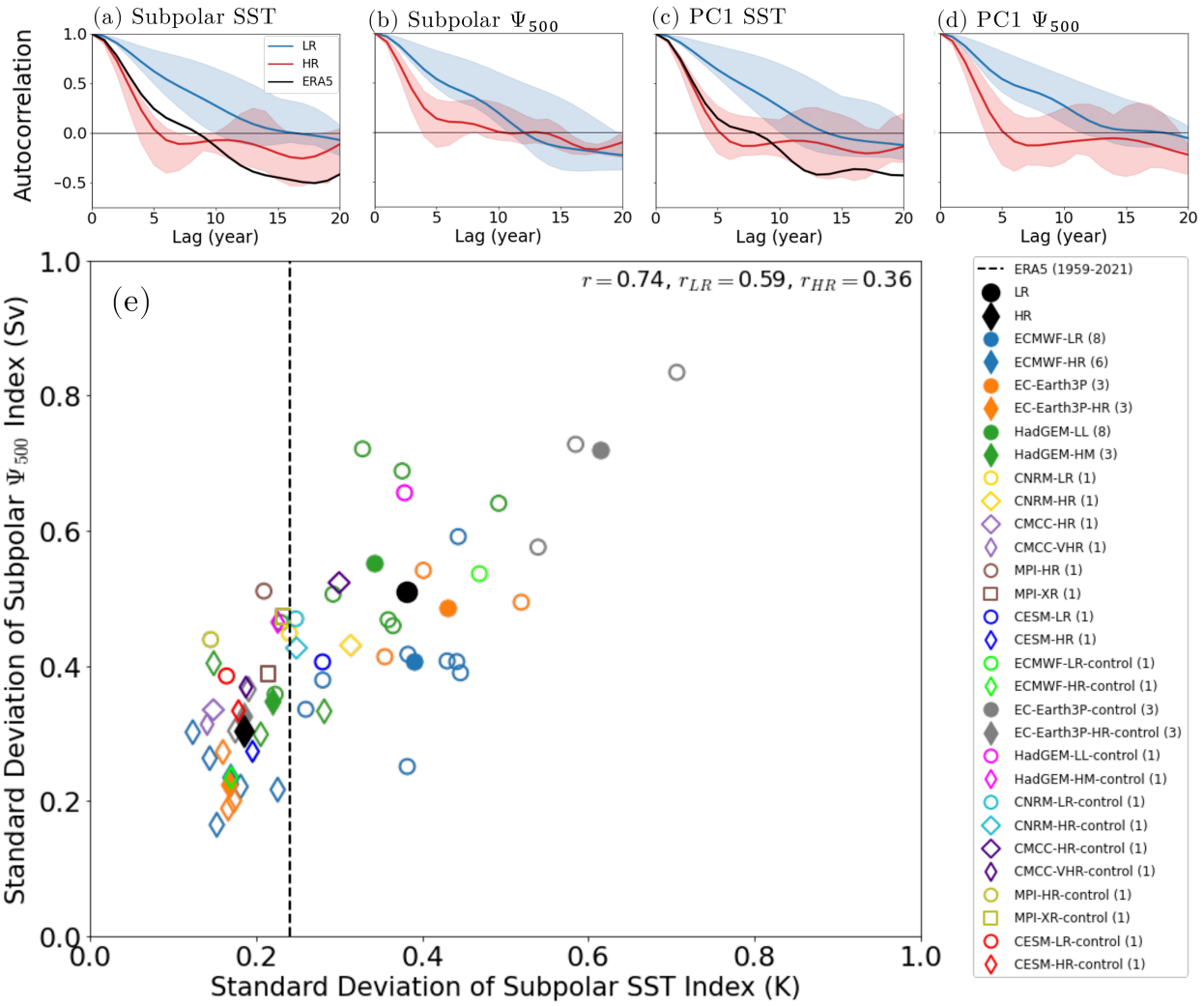

FIG. 5. Autocorrelation of (a) subpolar SST index and (b) subpolar Ψ_{500} index. Autocorrelations are calculated for ERA5 (SST only; black line) and for the multimodel ensemble mean of the LR control runs (blue lines) and HR control runs (red lines) with the associated spread across model runs (transparent shading). (c),(d) As in (a) and (b), but for the respective leading PCs. (e) Standard deviation of subpolar Ψ_{500} index (Sv; vertical axis) vs standard deviation of subpolar SST index (K; horizontal axis). Results are shown for individual members (unfilled markers) and ensemble means (filled markers) from all LR runs (circles) and HR runs (diamonds). The MR runs with high resolution in the ocean and low resolution in the atmosphere (i.e., CMCC-HR and CNRM-HR) are denoted by rotated square markers, and the MR runs with high resolution in the atmosphere and low resolution in the ocean (i.e., MPI-XR) are denoted by regular square markers. All indices were calculated from low-pass filtered anomalies.

et al. 2009), we calculated the lagged correlation between the NAO and the leading PCs of Ψ_{500} and SST (Fig. 6). However, we found no statistically significant lagged correlation between the NAO and PC1 of Ψ_{500} (Fig. 6b) nor with PC1 of SST (Fig. 6a) in the LR models. Therefore, the ocean circulation-driven subpolar SST variability in the LR models, as evidenced by the positive correlation between PC1 of Ψ_{500} and PC1 of SST (Fig. 6c; blue line), is not related to the NAO. In contrast, there is a statistically significant lagged correlation between the NAO and PC1 of Ψ_{500} in the HR models, which is consistent with previous studies showing that low-frequency variability in the Gulf Stream tends to lag the NAO by a few years (e.g., Frankignoul et al. 2001; Famooss Paolini et al. 2023, manuscript submitted to *J. Climate*). The correlation between the NAO and PC1 of SST also exhibits a similar peak at a lag of 1–2 years in the HR models and ERA5 (Fig. 6a), which is consistent with the improvement in the NAO–SST relationship in the HR models. Although ocean models with low resolution can simulate the Gulf Stream response to the NAO (e.g., de Coëtlogon et al. 2006), we found that the NAO has a stronger correlation with Ψ_{500} and SST anomalies averaged over the Gulf Stream region in the HR models compared to the LR models analyzed in this study (Fig. S2). This suggests that the NAO–Gulf Stream relationship is strengthened in the HR models, possibly from the effects of ocean eddies and atmosphere–ocean feedbacks that are either unresolved or misrepresented in

Brought to you by UNIV BOLOGNA-CAMPUS RAVENNA | Unauthenticated | Downloaded 02/14/24 03:05 PM UTC

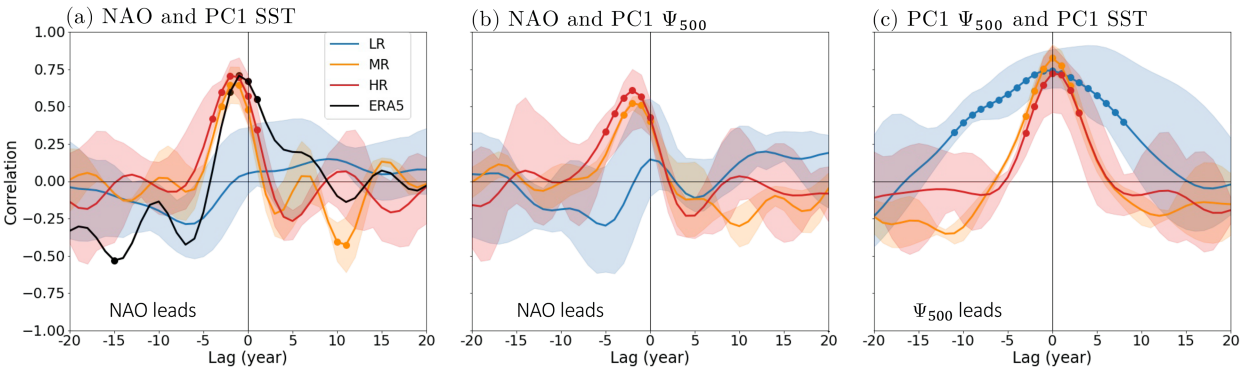

FIG. 6. Cross-correlation between low-pass filtered (a) NAO and leading PC of SST anomalies, (b) NAO and leading PC of Ψ_{500} anomalies, and (c) leading PC of Ψ_{500} and SST anomalies. In (a) and (b) negative lags indicate that the NAO leads the other indices, and in (c) negative lags indicate that Ψ_{500} leads SST. Correlations are calculated for the multimodel mean of the LR control runs (blue lines) and HR control runs (red lines) with the associated spread across model runs indicated by the transparent shading. Correlations for ERA5 are calculated in (a) only (black line). Correlations for the MR runs from ECMWF and HadGEM (see Table 1) are also shown in each panel (orange lines). Correlations that are found to be statistically significant (see section 2e) are indicated by round markers.

the LR models (e.g., Siqueira and Kirtman 2016; Bellucci et al. 2021; Famooss Paolini et al. 2022; Tsartsali et al. 2022).

Figure 6 indicates that the greater low-frequency variability of the ocean circulation in the LR models is related to ocean variability that is not directly driven by the NAO. It is also noted that PC1 of Ψ_{500} in the LR models is not related to significant SLP anomalies at any lag (not shown) and thus no atmospheric pattern seems involved. We refer to this non-atmospheric-driven variability as *intrinsic* ocean variability. Supporting the role of ocean processes, the improved NAO–SST–Ψ_{500} correlation in the HR models appears to be largely related to increased resolution in the ocean model component since the improvements are similar in the MR configurations of ECWMF and HadGEM (orange curves in Fig. 6), in which only the ocean resolution was increased.

b. AMOC

In this section, we explore whether the AMOC plays a role in the overestimated intrinsic subpolar ocean variability in the LR models, since previous modeling studies have reported AMOC-related SST variability in the subpolar region at low-frequency time scales (e.g., Zhang 2008; Ba et al. 2014; Muir and Fedorov 2015; Buckley and Marshall 2016), as well as substantial intrinsic variability in the AMOC (e.g., Delworth and Zeng 2012; Jiang et al. 2021; Liu and Fedorov 2022; Meccia et al. 2023; Wei and Zhang 2022).

1) SALINITY- VERSUS TEMPERATURE-CONTROLLED UPPER-OCEAN DENSITY ANOMALIES

The analysis of the AMOC is first motivated by discussing the upper-ocean density (i.e., depth-integrated between 0 and 500 m; ρ_{500}) and MLD anomalies associated with subpolar ocean variability since MLD anomalies are related to variability in oceanic convection and ρ_{500} anomalies are related to buoyancy-driven variability in the ocean circulation and hence the AMOC (e.g., Yeager and Danabasoglu 2014; Ortega et al. 2017, 2021). We estimated the observed ρ_{500} from upper-ocean salinities and temperatures using EN4 data, but we did not estimate observed MLDs from EN4 because ocean observations at greater depths are sparse before the year 2000 when Argo floats were not available (Koenigk et al. 2021) and hence this would contribute to substantial uncertainty in the low-frequency variability of the observed estimate of MLDs.

Strikingly, the patterns for ρ_{500} and MLD regressed onto the subpolar SST index are roughly opposite between the LR and HR models (Figs. 7b–g). The LR models exhibit warm subpolar SSTs together with positive ρ_{500} anomalies and MLD deepening (red contours) in the Labrador–Irminger Seas, whereas the HR models exhibit warm subpolar SSTs together with negative ρ_{500} anomalies and MLD shallowing (blue contours) in this region. The pattern of ρ_{500} anomalies in the HR models also appears more realistic, as it is more consistent with the ρ_{500} pattern derived from EN4 observations (Fig. 7a).

Since warm SSTs act to reduce ρ_{500}, the subpolar temperature anomalies cannot be the driver of the positive ρ_{500} anomalies in the subpolar region in the LR models, where ρ_{500} anomalies and convection (MLD deepening) must be driven by upper-ocean salinity anomalies. This is opposite to the HR models where the subpolar ρ_{500} anomalies and convection (MLD shallowing) seem to be driven by upper-ocean temperature anomalies. Indeed, Figs. 7h–n show that subpolar SST variability is associated with salinity-related ρ_{500} anomalies ($\rho_{S,500}$; pink shading) in the LR models, whereas subpolar SST variability is associated with temperature-related ρ_{500} anomalies ($\rho_{T,500}$; green shading) in the HR models and observations.

Why are subpolar ρ_{500} anomalies related to salinity in the LR models, but to temperature in the HR models and in observations? To explain this central result, we turn to a key study by Menary et al. (2015a), which revealed a strong correlation between CMIP5 biases in the salinity control versus

Brought to you by UNIV BOLOGNA-CAMPUS RAVENNA | Unauthenticated | Downloaded 02/14/24 03:05 PM UTC

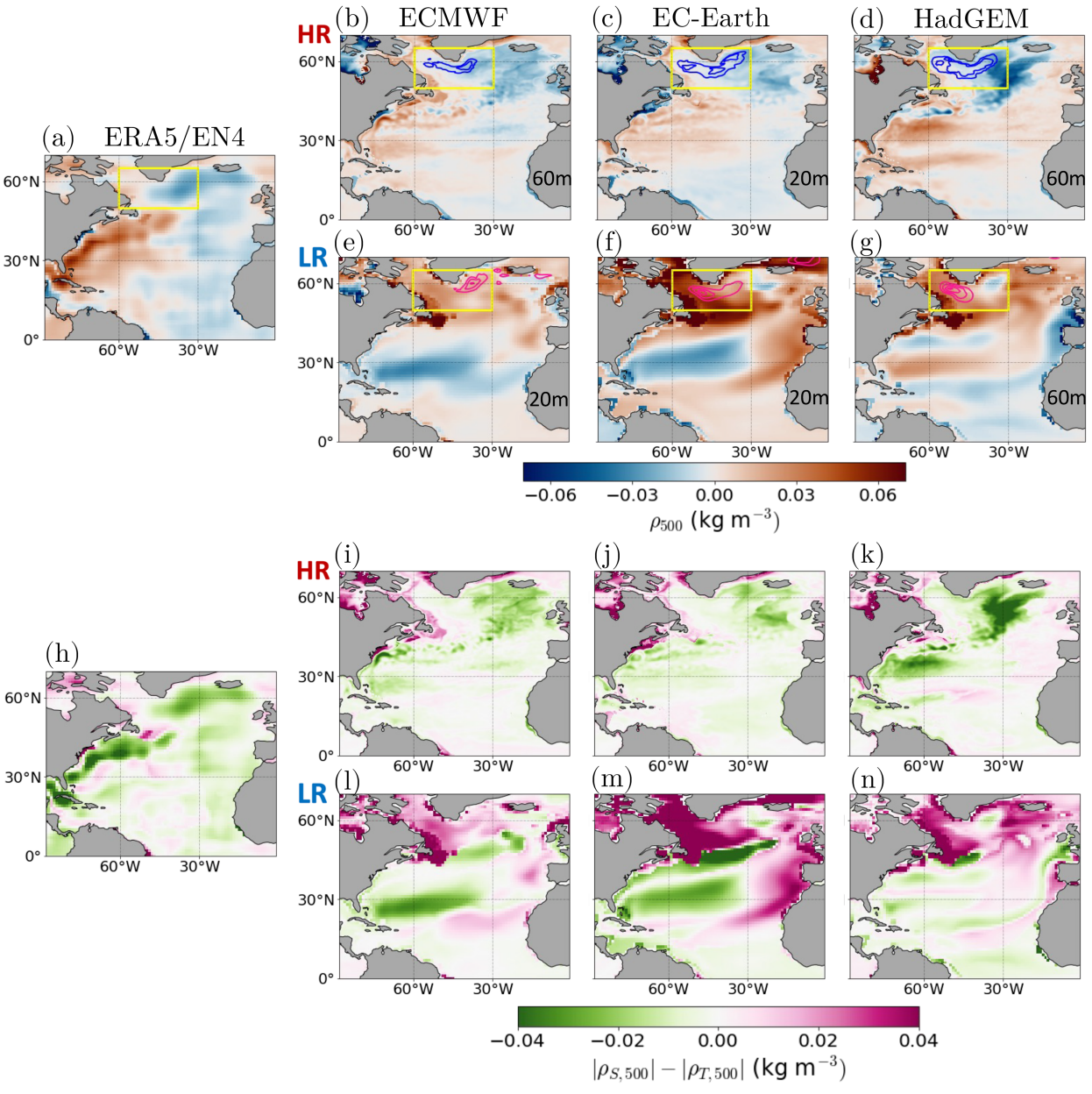

FIG. 7. Upper-ocean density (ρ_{500}) anomalies regressed onto the standardized subpolar SST index (shading; kg m^{-3}) for (a) ρ_{500} anomalies calculated from EN4 observations and the subpolar SST index calculated from ERA5, (b)–(d) the HR control runs, and (e)–(g) the LR control runs. In (b)–(g), MLD anomalies regressed onto the standardized subpolar SST index are also shown (contours; m). The MLD contour interval is indicated in the lower-right side of each panel. Positive MLD anomalies are indicated by red contours and negative MLD anomalies are indicated by blue contours. (h)–(n) As in (a)–(g), but for the difference in magnitudes of the salinity component of ρ_{500} anomalies ($\rho_{S,500}$) and temperature component of ρ_{500} anomalies ($\rho_{T,500}$) regressed onto the standardized subpolar SST index (shading; kg m^{-3}). All fields were low-pass filtered before calculating the regressions.

temperature control of ρ_{500} anomalies in the Labrador Sea to biases in mean salinity and temperature in this region. As discussed in Menary et al. (2015a), this can be explained by the nonlinearity of the equation of state for seawater. In particular, salinity perturbations have a greater impact on density when the mean temperature is cooler and mean salinity is lower, whereas temperature perturbations have a greater impact on density when the mean temperature is warmer and the salinity is higher (see Fig. S3 for an illustrative case).

Considering this dependence, Figs. 8a and 8b explore whether the models in this study exhibit a relationship between mean upper-ocean salinity (S_{500}) and temperature (T_{500}) biases in the Labrador–Irminger Seas and the salinity versus temperature control of ρ_{500} anomalies ($\rho_{\text{SvsTcontrol}}$; defined in section 2f)

Brought to you by UNIV BOLOGNA-CAMPUS RAVENNA | Unauthenticated | Downloaded 02/14/24 03:05 PM UTC

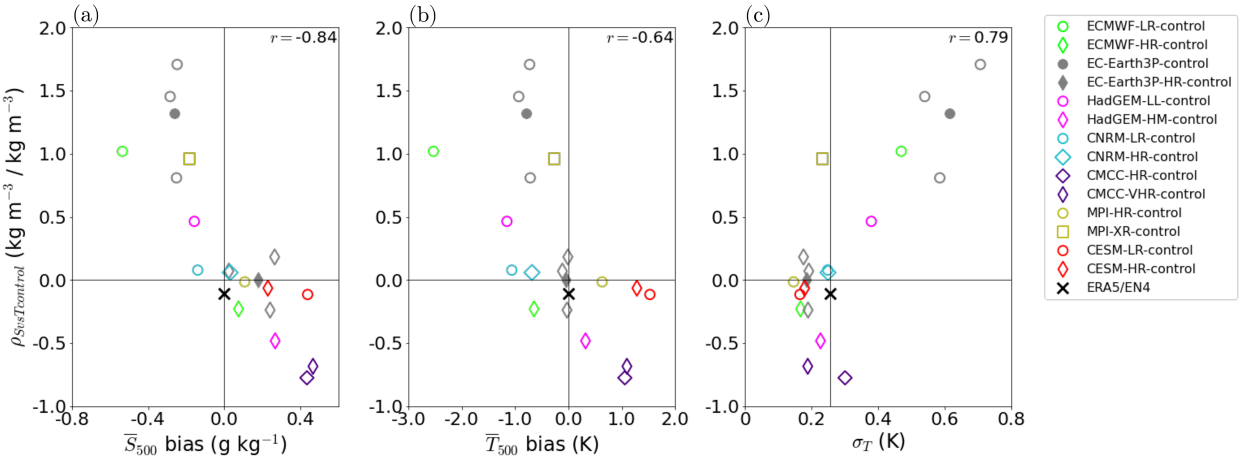

FIG. 8. (a) The climatological mean bias in upper-ocean salinity (S_{500}; g kg^{-1}) averaged over the Labrador–Irminger Seas (50°–65°N, 30°–60°W) vs the salinity vs temperature control of low-pass filtered ρ_{500} anomalies ($\rho_{SvTcontrol}$; kg m^{-3} kg^{-1} m^{-3}) averaged over the same region. Results are calculated for all control runs with markers following the same labeling convention as Fig. 5e. (b) As in (a), but for the climatological mean upper-temperature (T_{500}) bias averaged over the Labrador–Irminger seas (K). (c) As in (a), but for the standard deviation of the low-pass filtered subpolar SST index (K).

averaged over this region (yellow box in Fig. 7). Indeed, the models considered here exhibit convection anomalies in this region in association with subpolar SST variability, and hence this is a key region for linking the AMOC with subpolar SST variability in these simulations. This is also generally the case for CMIP5 models (Ortega et al. 2021), but there is ongoing debate regarding the precise location of deep convection in the North Atlantic and its links to the AMOC in reality (Lozier et al. 2019; Petit et al. 2020; Menary et al. 2020; Megann et al. 2021; Yeager et al. 2021). Note that maps of multimodel mean S_{500} and T_{500} biases are shown in Fig. S4.

Consistent with Menary et al. (2015a), Figs. 8a and 8b show a significant negative correlation between $\rho_{SvsTcontrol}$ and mean S_{500} bias ($r = -0.84$) as well as mean T_{500} bias ($r = -0.64$) in this region. The LR models also generally exhibit colder and fresher Labrador–Irminger Seas and salinity-controlled density anomalies ($\rho_{SvsTcontrol} > 0$), whereas the HR models and EN4 observations exhibit warmer and saltier Labrador–Irminger Seas and temperature-controlled density anomalies ($\rho_{SvsTcontrol} < 0$). The main exceptions are the LR configurations of CESM and MPI, which are more like the HR models with warmer and saltier Labrador–Irminger Seas. It is also noted that Menary et al. (2015a) showed that $\rho_{SvsTcontrol}$ is positive (salinity-controlled density anomalies) for EN4 observations averaged over the Labrador Sea. We also find that $\rho_{SvsTcontrol}$ is positive in the Labrador Sea, but that $\rho_{SvsTcontrol}$ is negative in the Irminger Sea and exceeds the positive contribution from the Labrador Sea when averaging over both regions.

Figure 8c shows that $\rho_{SvsTcontrol}$ is also correlated with the amplitude of subpolar SST variability across all control runs ($r = 0.79$). Furthermore, the LR models tend to have the largest standard deviation in the subpolar SST index and salinity-controlled ρ_{500} anomalies, whereas the HR models and observations indicate a lower standard deviation in the subpolar SST index and temperature-controlled ρ_{500} anomalies. Exceptions to this behavior are the LR configurations of CNRM, MPI, and CESM, which are more similar to the HR models. It is also noted that the relationship between subpolar SST variance and $\rho_{SvsTcontrol}$ appears to be asymmetric. In particular, models with $\rho_{SvsTcontrol} \leq 0$ have similar small amplitudes of subpolar SST anomalies that are essentially uncorrelated with $\rho_{SvsTcontrol}$, whereas models with $\rho_{SvsTcontrol} > 0$ appear to exhibit larger amplitudes of subpolar SST anomalies that are positively correlated with $\rho_{SvsTcontrol}$.

Finally, note that Fig. 8 was produced from the control runs, but qualitatively similar results were found for the historical runs, except with weaker correlations between variables (e.g., $r = -0.61$ for $\rho_{SvsTcontrol}$ and mean S_{500}, and $r = 0.58$ for $\rho_{SvsTcontrol}$ and the standard deviation of subpolar SSTs). The weaker correlations could be due to the spread in $\rho_{SvsTcontrol}$ among members over the 65-yr historical simulation period and/or the imperfect removal of the global warming signal from $\rho_{SvsTcontrol}$.

2) SALINITY- VERSUS TEMPERATURE-CONTROLLED AMOC

In this section, we argue that the salinity control of subpolar ρ_{500} anomalies in LR models versus temperature control of ρ_{500} anomalies in HR models affects the variability of the AMOC by favoring different feedbacks.

The AMOC transports both heat and salinity into the North Atlantic subpolar region (e.g., Buckley and Marshall 2016; Johnson et al. 2019). As such, a positive AMOC anomaly leads to additional heat transport into the subpolar ocean, which reduces upper-ocean density in this region, and hence may eventually reduce deep convection and dampen the initial AMOC anomaly. However, a positive AMOC anomaly also leads to additional salinity transport into the subpolar region, which increases upper-ocean density in this region, and hence may eventually enhance convection and reinforce the

Brought to you by UNIV BOLOGNA-CAMPUS RAVENNA | Unauthenticated | Downloaded 02/14/24 03:05 PM UTC

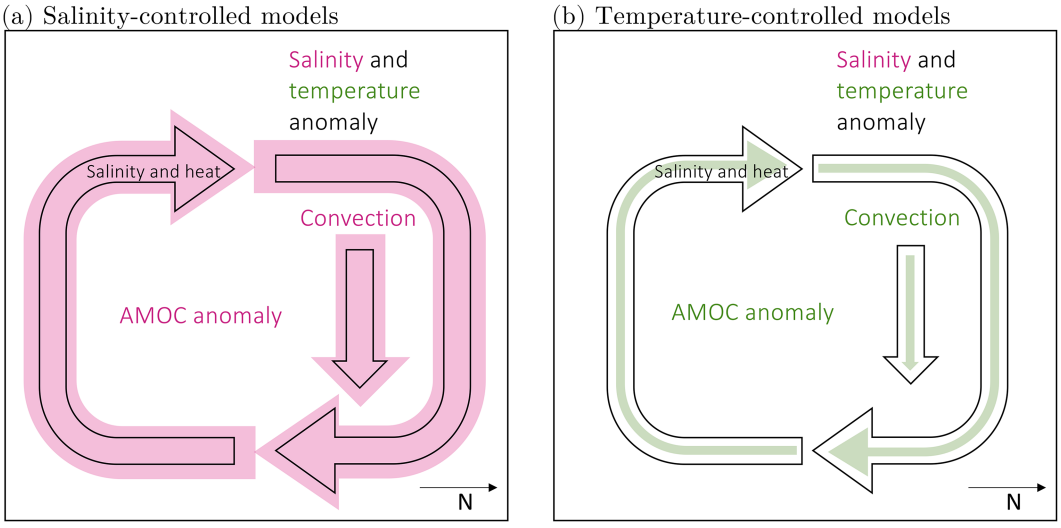

FIG. 9. Schematic of (a) positive feedback between the AMOC and upper-ocean salinity and (b) negative feedback between the AMOC and upper-ocean temperature, as described in the text. The black arrows indicate a positive AMOC anomaly, and the colored arrows illustrate the effect of the positive or negative feedback on the amplitude of the AMOC anomaly as indicated by the width of the arrows. (a) In models that have a greater salinity control of subpolar ocean density anomalies, there is a strengthening of convection and an amplification of the initial AMOC anomaly (purple arrows). (b) In models that have a greater temperature control of subpolar ocean density anomalies, there is a weakening of convection and a dampening of the initial AMOC anomaly (green arrows).

initial AMOC anomaly. Therefore, such AMOC–salinity interactions can lead to a positive feedback on subpolar ocean variability, whereas such AMOC–temperature interactions can lead to a negative feedback on subpolar ocean variability, as suggested by previous studies (e.g., Frankignoul et al. 2009; Delworth and Zeng 2012; Kwon and Frankignoul 2014; Menary et al. 2015b; Ortega et al. 2017; Reintges et al. 2017; Oldenburg et al. 2021).

Here we adopt the following hypotheses:

1) The positive feedback between subpolar upper-ocean salinity anomalies and the AMOC is favored in models that have a greater salinity control of subpolar ρ_{500} anomalies (i.e., LR models), as illustrated in Fig. 9a.
2) The negative feedback between subpolar upper-ocean temperature anomalies and the AMOC is favored in models that have a greater temperature control of subpolar ρ_{500} anomalies (i.e., HR models), as illustrated in Fig. 9b.

The first piece of supporting evidence for our hypotheses is provided in Fig. 10a, which shows the standard deviation of low-pass filtered overturning circulation anomalies (Ψ_V) averaged over 40°–60°N calculated using the LR and HR control runs from ECMWF, EC-Earth, and HadGEM. The results clearly indicate that the LR models considered here, and hence the same models that exhibit salinity-controlled density anomalies in the subpolar region (Figs. 7 and 8) exhibit greater low-frequency variance in the AMOC. This is consistent with a stronger positive feedback acting on the AMOC in the LR models and a stronger negative feedback acting on the AMOC in the HR models.

To connect the findings here to those related to the horizontal upper-ocean circulation (Ψ_{500}), Fig. 10b shows that the standard deviation of the AMOC index is positively correlated with that of the subpolar Ψ_{500} index across all control runs ($r = 0.77$; the correlation decreases to $r = 0.62$ when also considering the historical runs). The associated salinity control versus temperature control of ρ_{500} anomalies in the Labrador–Irminger Seas ($\rho_{\mathrm{SvsTcontrol}}$) for each run is also indicated by the color of each marker (see Fig. S5 for markers that are colored by the model name instead of $\rho_{\mathrm{SvsTcontrol}}$). Clearly, the model runs with low oceanic resolution generally have larger variance in both indices *and* a greater salinity control of ρ_{500} anomalies (circle markers are darker purple) compared to model runs with high oceanic resolution (diamond markers are green/lighter purple). Note that the coupling between the subpolar gyre and AMOC is expected from previous studies (e.g., Larson et al. 2020; Ortega et al. 2021) and is understood to arise from torque exerted by bottom topography (Yeager and Danabasoglu 2014; Yeager 2015). The relationship between the subpolar horizontal circulation and the AMOC is also supported by correlations between respective indices of variability used in our study (not shown), but with stronger correlations for the LR models in agreement with results from Meccia et al. (2021). This could be due to the stronger positive feedback in the LR models, which may enhance the correlation between oceanic variables in the subpolar region.

Further supporting evidence for our hypotheses is provided in Fig. 11, which shows multimodel mean cross-correlations between the AMOC index and different variables averaged over the subpolar region (45°–65°N, 5°–60°W) using the LR and HR control runs from the three models. The variables correlated

Brought to you by UNIV BOLOGNA-CAMPUS RAVENNA | Unauthenticated | Downloaded 02/14/24 03:05 PM UTC

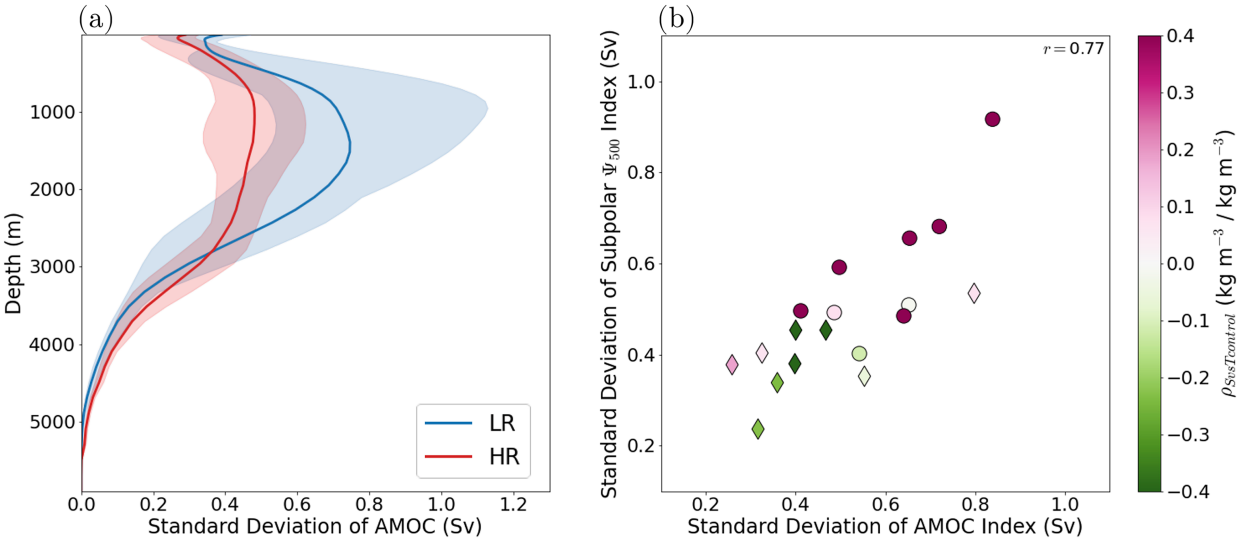

FIG. 10. (a) Standard deviation of low-pass filtered overturning streamfunction anomalies Ψ_V (Sv) averaged over 40°–60°N. The multimodel mean standard deviation is calculated from the LR control runs (blue line) and HR control runs (red line) with the associated spread across model runs indicated by transparent shading. (b) Standard deviation of low-pass filtered subpolar Ψ_{500} index (vertical axis; Sv) vs standard deviation of the low-pass filtered AMOC index (horizontal axis; Sv) as defined in section 2d for all control runs with high resolution in the ocean model (circle markers) and low resolution in the ocean model (diamond markers). The color of each marker indicates the salinity vs temperature control of ρ_{500} anomalies ($\rho_{\mathrm{SvTcontrol}}$) averaged over the Labrador–Irminger Seas.

with the AMOC index include S_{500} and SST anomalies, as well as MLD and ρ_{500} anomalies. Note that qualitatively similar relationships are found for averages over the western portion of the subpolar region (i.e., the Labrador–Irminger Seas).

The lead–lag correlations shown in Fig. 11 are highly consistent with a positive feedback between the AMOC and upper-ocean salinity in the LR models and a negative feedback between the AMOC and SST in the HR models. In particular, in the LR models, a positive AMOC anomaly is associated with positive subpolar ρ_{500} and MLD anomalies (enhanced convection) at all lags (Figs. 11a,b), which acts to reinforce the initial AMOC anomaly. However, in the HR models, a positive AMOC anomaly leads to negative subpolar ρ_{500} and MLD anomalies (reduced convection), which acts to damp the initial AMOC anomaly and hence contributes to the marked asymmetrical lead–lag correlations. Clearly, the asymmetrical lead–lag correlations in the HR models are related to subpolar SST anomalies (Fig. 11d), whereas the positive correlations between the AMOC and ρ_{500} anomalies in LR models must be related to subpolar salinity anomalies (Fig. 11c). Indeed, this is supported by cross-correlations between the AMOC and temperature- or salinity-related components of ρ_{500} (Fig. S6). Overall, the positive and negative AMOC feedback that is favored in the LR and HR models, respectively, is consistent with the longer time scale of subpolar ocean variability in the LR models compared to the HR models.

c. *Possible causes of mean biases in the Labrador–Irminger Seas*

Previous studies have suggested that mean biases in upper-ocean temperatures and salinities in the subpolar ocean could be related to the mean strength of the ocean circulation, with lower-resolution models generally having a weaker mean AMOC and weaker poleward heat and salinity transport, and hence a colder and fresher subpolar ocean compared to higher-resolution models (Docquier et al. 2019; Roberts et al. 2019; Hewitt et al. 2020). These biases have also been suggested to arise from the simulated orientation of the North Atlantic Current, which tends to be too zonal in lower-resolution models (e.g., Wang et al. 2014; Marzocchi et al. 2015; Drews and Greatbatch 2016; Danabasoglu et al. 2016; Jackson et al. 2020). Additionally, it has been argued that high-resolution models may have excessive deep convection in the Labrador Sea (Roberts et al. 2019; Koenigk et al. 2021), and hence the overestimated downwelling in this region could contribute to the warm and salty bias found in some of these models (Figs. 8a,b and Fig. S3).

While a comprehensive diagnosis of the causes of the mean biases in the Labrador–Irminger Seas is beyond the scope of this paper, we found that the maximum of the climatological mean AMOC calculated over the extratropical North Atlantic domain is positively correlated with the mean S_{500} ($r = 0.73$) and mean T_{500} ($r = 0.84$) in the Labrador–Irminger Seas across all control runs (Figs. 12a,b). The maximum magnitude of the climatological mean Ψ_{500} calculated over the subpolar region was found to be even more strongly correlated with the mean S_{500} ($r = 0.90$) and similarly correlated with the mean T_{500} ($r = 0.82$) in the Labrador–Irminger Seas, with LR models generally having a weaker mean subpolar Ψ_{500} than HR models (Figs. 12c,d). This is also illustrated in Fig. 4, which shows weaker mean Ψ_{500} (contours) in the subpolar region in the LR configurations of ECMWF, EC-Earth, and HadGEM compared to their respective HR configurations. Interestingly, the LR configurations of MPI and CESM are exceptions to this, both having a stronger mean AMOC and

Brought to you by UNIV BOLOGNA-CAMPUS RAVENNA | Unauthenticated | Downloaded 02/14/24 03:05 PM UTC

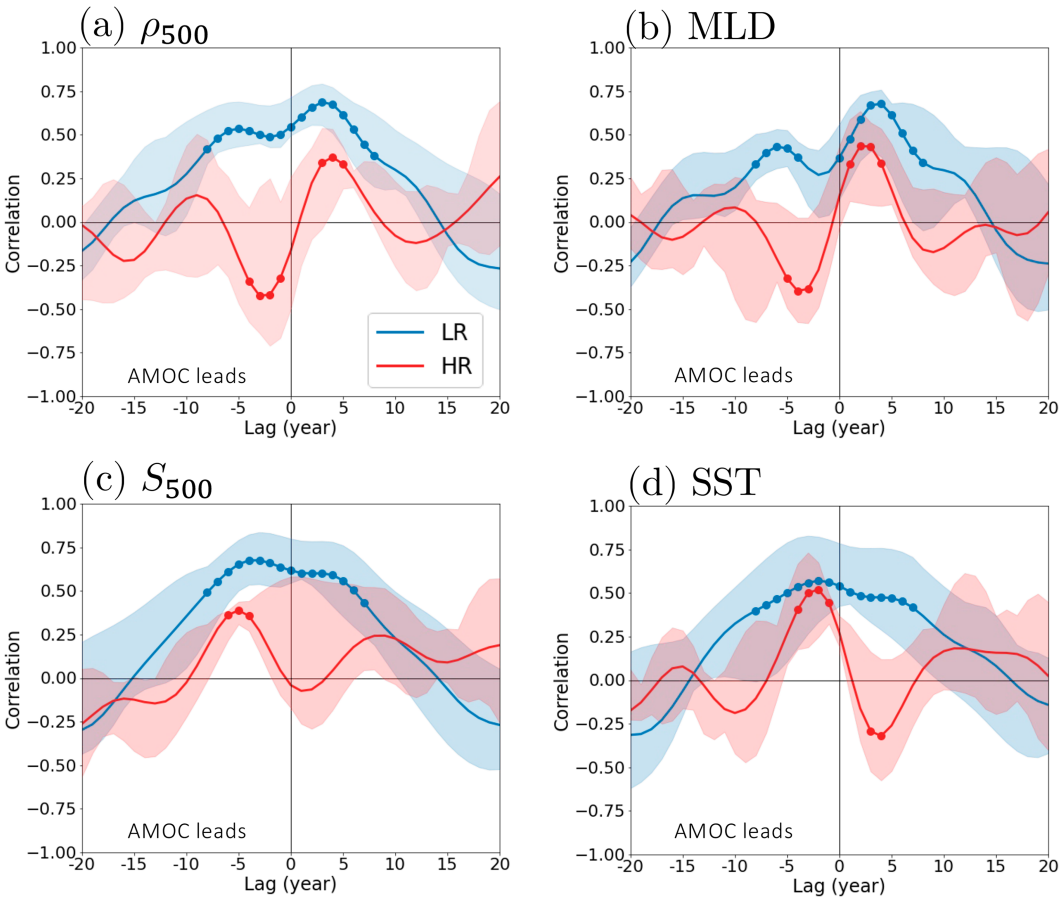

FIG. 11. Cross-correlation between low-pass filtered AMOC index and variables averaged over the broader subpolar region (45°–65°N, 5°–60°W), including (a) upper-ocean density anomalies (ρ_{500}), (b) mixed layer depth (MLD), (c) upper-ocean salinity (S_{500}), and (d) SST. Negative lags indicate that the AMOC index leads the other variables. Multimodel mean correlations are calculated from the LR control runs (blue lines) and HR control runs (red lines) with the associated spread across model runs indicated by transparent shading. Also shown in (a) are the multimodel mean correlations calculated from all control runs with a greater salinity control of ρ_{500} anomalies in the Labrador–Irminger Seas (purple line) and a greater temperature control of ρ_{500} anomalies in the Labrador–Irminger Seas (green line). Correlations that are found to be statistically significant (see section 2e) are indicated by round markers.

subpolar Ψ_{500} compared to other LR models. This could also explain why these models appear to have warmer and saltier Labrador–Irminger Seas and temperature-controlled density anomalies in this region (Figs. 8a,b).

5. Concluding discussion

In this study, we assessed the impacts of increased horizontal model resolution on the representation of atmosphere–ocean variability in the North Atlantic using multimodel output from HighResMIP. The following were found:

1) Some of the models with low horizontal resolution (i.e., the LR configurations of ECMWF, EC-Earth, and HadGEM) overestimate the low-frequency SST anomalies in the subpolar region and underestimate their correlation with the NAO (e.g., Figs. 1 and 2)
2) The bias in extratropical atmosphere–ocean variability is largely reduced when the ocean resolution is increased from ~1.0° to ~0.25°, and the improvements are primarily related to a reduction in intrinsic (i.e., non-NAO-driven) variability of the ocean circulation (e.g., Figs. 5 and 6)
3) The LR models with excessive subpolar SST variability also have colder and fresher mean state in the Labrador–Irminger Seas and a greater salinity control of density anomalies in this region compared to the EN4 observational product and the HR models, which generally exhibit a greater temperature control of density anomalies in this region (e.g., Fig. 8).

We hypothesized that the third finding favors 1) a positive feedback between the AMOC and subpolar upper-ocean salinity in the LR models (Fig. 9a) and 2) a negative feedback between the AMOC and subpolar SST in the HR

Brought to you by UNIV BOLOGNA-CAMPUS RAVENNA | Unauthenticated | Downloaded 02/14/24 03:05 PM UTC

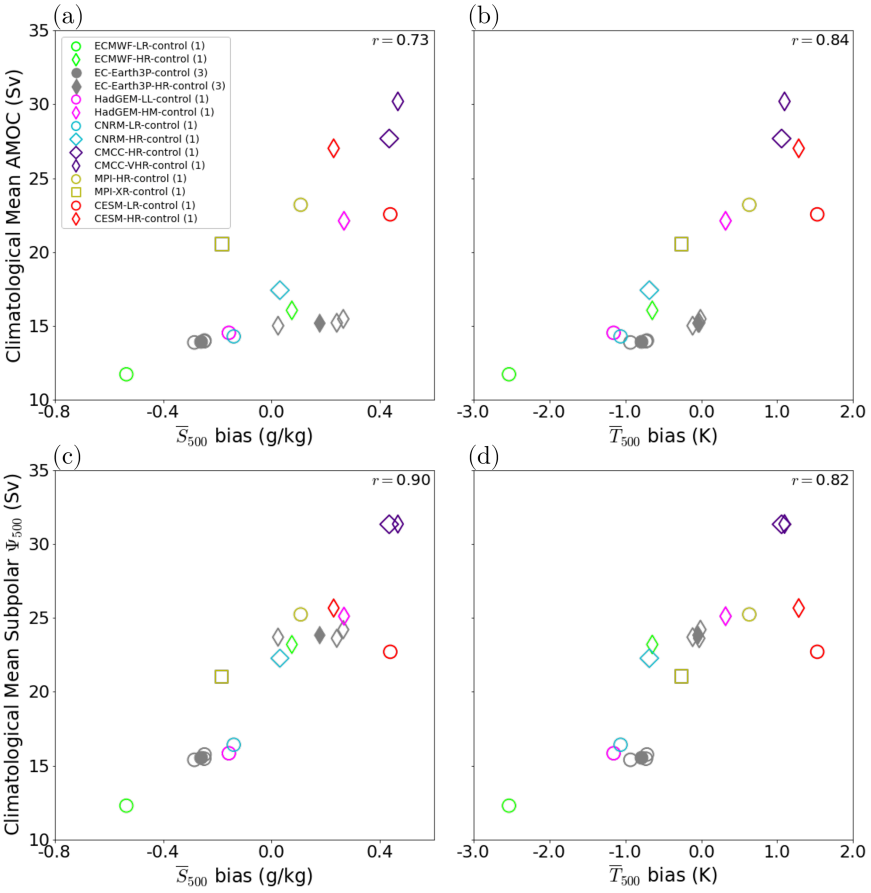

FIG. 12. Maximum of the climatological mean overturning circulation field (Sv) calculated over 30°–60°N and 500–2000 m depth vs the (a) mean bias in upper-ocean salinity (S_{500}; K) averaged over the Labrador–Irminger Seas. Results are shown for all control runs using the same labeling convention as in Fig. 8a. (b) As in (a), but for the mean bias in upper-ocean temperature (T_{500}; g kg^{-1}). (c),(d) As in (a) and (b), but for the maximum magnitude of the climatological mean Ψ_{500} field calculated over the subpolar North Atlantic region (45°–65°N, 5°–60°W).

models (Fig. 9b). Supporting evidence included the greater low-frequency variance of the AMOC in the LR models compared to the HR models (Fig. 10) and lead–lag correlations between the AMOC and subpolar SST, upper-ocean salinity, and density anomalies that differ between the LR and HR models (Fig. 11). Since the AMOC–salinity feedback enhances subpolar ocean variability independently of the atmospheric circulation and the AMOC–temperature feedback damps variability of the ocean circulation, we argue that these mechanisms are ultimately responsible for the overestimated intrinsic subpolar ocean variability in the LR models and the stronger, more realistic relationship between the NAO and SSTs in the HR models.

While our results indicate a weaker role for the AMOC and relatively stronger role for NAO forcing of SST anomalies in the HR models compared to the LR models, they also seem to suggest that some aspects of the ocean circulation become more strongly linked to the NAO with increased model resolution, particularly the Gulf Stream. The stronger NAO–Gulf Stream relationship in HR models could be related to the effects of ocean eddies and atmosphere–ocean interactions that are either unresolved or misrepresented in the LR models (e.g., Siqueira and Kirtman 2016; Famooss Paolini et al. 2022). Further studies are needed to better understand how model resolution impacts the complex interactions between the NAO and the ocean circulation.

Our findings are broadly consistent with previous modeling studies showing that salinity anomalies play an important role in North Atlantic variability in coarse-resolution models (e.g., Delworth et al. 1993; Frankignoul et al. 2009; Delworth and Zeng 2012; Ba et al. 2014; Menary et al. 2015a; Jiang et al. 2021; Lai et al. 2022; Liu et al. 2022; Meccia et al. 2023) and seemingly less important role in higher-resolution models (e.g., Menary et al. 2015a; Lai et al. 2022). In particular, Menary et al. (2015a) showed that subpolar upper-ocean density variability in CMIP5 models is more closely related to salinity

Brought to you by UNIV BOLOGNA-CAMPUS RAVENNA | Unauthenticated | Downloaded 02/14/24 03:05 PM UTC

anomalies in lower-resolution models versus temperature anomalies in higher-resolution models due to differing mean states of the Labrador Sea. Consistently, Ba et al. (2014) showed that AMOC variability is salinity driven in centennial to millennial-year-long LR simulations and suggested that this may be related to cold and fresh biases in the subpolar ocean. Lai et al. (2022) also showed that salinity played an important role in driving AMV and AMOC variability in a LR configuration of HadGEM, while NAO-related surface heat fluxes played a more important role in its HR configuration. However, our findings are seemingly inconsistent with some studies that argued that the mechanisms of AMOC variability are relatively insensitive to model resolution (e.g., Oldenburg et al. 2021, 2022). This may be because not all models exhibit large changes with increasing resolution in the mean ocean circulation and hence also in upper-ocean temperature and salinity in the subpolar region, as indeed is the case for CESM (Figs. 8a,b and 12). This is expected as the mean ocean circulation is also affected by other physics that may vary across models.

Some of our key results seem inconsistent with Menary et al. (2015a), who reported no systematic relationship between the time scales of North Atlantic variability simulated by CMIP5 models and the salinity versus temperature control of density anomalies in the Labrador Sea. The reasons for this apparent discrepancy could be due to their focus on periodicity rather than persistence or amplitude of the low-frequency variability, their analysis of primarily lower-resolution models, and/or our more limited sample of models. Furthermore, while our finding that the LR models from HighResMIP tend to overestimate the low-frequency variance of extratropical North Atlantic SSTs is consistent with some prior studies (e.g., Ba et al. 2014; Danabasoglu et al. 2016), it conflicts with other studies showing that coarse-resolution models generally underestimate AMV (e.g., Cheung et al. 2017; Murphy et al. 2017; Yan et al. 2018). These discrepancies could be due to differences in the analyzed time scale, and also model-to-model differences. Indeed, we have argued that model diversity in the amplitudes of subpolar SST variability may be partly related to model diversity in the mean state of the subpolar region (e.g., CESM-LR has warmer and saltier Labrador–Irminger Seas with lower subpolar SST variance, while ECMWF-LR has colder and fresher Labrador–Irminger Seas with greater subpolar SST variance). It would be useful to assess the impacts of resolution in a more diverse collection of climate models, since the majority of the models analyzed here use the same ocean model component (NEMO) and the two models that use a different ocean model component (i.e., MPI and CESM) behave differently.

Although we focused on the role of salinity and temperature advection by the AMOC and its feedback effects in the LR and HR models, differences in damping processes may contribute to differences in subpolar ocean variability between the LR and HR models. In particular, salinity anomalies are expected to have weaker local damping rates compared to temperature anomalies because salinity anomalies are damped only by ocean processes (e.g., vertical mixing and entrainment), whereas temperature anomalies are damped both by surface heat fluxes and ocean processes (Hall and Manabe 1997; Frankignoul et al. 2002; Zhang et al. 2017). Thus, we expect that the salinity-controlled variability in the LR models is more weakly damped than the temperature-controlled variability in the HR models and hence may also contribute to the greater persistence of subpolar variability in LR models.

Uncertainty in the low-frequency variability of the ocean circulation over the observed record (e.g., Karspeck et al. 2017; Jackson et al. 2019) prevents us from making definitive conclusions about the realism of the simulated mechanisms of AMOC variability. However, our results suggest that the AMOC is *less* salinity-controlled and *more* temperature-controlled in reality compared to those low-resolution models that substantially overestimate subpolar SST variability. This hypothesis seems consistent with observation-based evidence from Chafik et al. (2022) suggesting that enhanced overturning is related to subpolar surface heat loss and positive density anomalies associated with a positive NAO. However, this does not necessarily imply that salinity does not play an important role in AMOC variability in reality. In fact, Menary et al. (2016) showed that Labrador Sea density anomalies are controlled by salinity in observations, and further showed that model hindcasts with an unrealistic temperature control of density anomalies in this region lead to poor skill in predicting the AMOC. In general, the primary mechanisms that drive variability in the AMOC and the subpolar ocean remain incompletely understood (e.g., Buckley and Marshall 2016; Zhang et al. 2019; Lozier et al. 2019; Petit et al. 2020; Menary et al. 2020; Jackson et al. 2022). This emphasizes the critical need for continued and improved ocean observations.

Overall, our results suggest that an improved representation of the climatological mean upper-ocean salinity and temperature in the subpolar region and hence mean ocean circulation in the North Atlantic could lead to substantial improvements in the simulated extratropical North Atlantic atmosphere–ocean variability on decadal to multidecadal time scales. Indeed, studies have shown that aspects of AMV can be improved by correcting for biases in mean sea surface salinity (Park et al. 2016) and the orientation of the North Atlantic Current (Drews and Greatbatch 2016). Furthermore, while we have argued that oceanic resolution plays a relatively more important role than atmospheric resolution in explaining the improvements in North Atlantic atmosphere–ocean variability with increasing model resolution in the HighResMIP models, previous studies have reported improvements in aspects of the extratropical atmospheric circulation with increasing model resolution (e.g., Siqueira and Kirtman 2016; Menary et al. 2018; Athanasiadis et al. 2022; Famooss Paolini et al. 2022). Hence, further studies are needed to better understand how such improvements may relate to coupled atmosphere–ocean processes. Last, as low-frequency anomalies in subpolar ocean heat content and SSTs are generally skillfully predictable by initialized LR decadal prediction systems (e.g., Yeager and Robson 2017; Borchert et al. 2021; Carmo-Costa et al. 2022), it remains to be understood how the subpolar ocean biases and their apparent resolution dependencies highlighted in this study may influence decadal climate predictions in the North Atlantic sector (e.g., Menary and Hermanson 2018; Robson et al. 2018).

Brought to you by UNIV BOLOGNA-CAMPUS RAVENNA | Unauthenticated | Downloaded 02/14/24 03:05 PM UTC

Acknowledgments. CRP and PJA acknowledge funding from the Italian Ministry of Education, University and Research (MIUR) through the JPI Oceans and JPI Climate "Next Generation Climate Science in Europe for Oceans" ROADMAP Project (D.D. n.1316, 8 June 2021). CF acknowledges funding from the JPI Oceans and JPI Climate Joint Call 2019 "Next Generation Climate Science in Europe for Oceans" ROADMAP Project, and partial support from NOAA MAP Grant NA21OAR431034.

Data availability statement. Monthly model output from HighResMIP can be found on Earth System Grid Federation (ESGF): https://esgf-node.llnl.gov/search/cmip6/. Monthly data from ERA5 data are available on the Climate Data Store (CDS): https://cds.climate.copernicus.eu/cdsapp#!/dataset/reanalysis-era5-single-levels?tab=overview. Salinity and temperature observations from EN4 (objective analyses, version 4.2.2) are available from the Met Office Hadley Centre (MOHC): https://www.metoffice.gov.uk/hadobs/en4/download-en4-2-2.html.

REFERENCES

Årthun, M., T. Eldevik, E. Viste, H. Drange, T. Furevik, H. L. Johnson, and N. S. Keenlyside, 2017: Skillful prediction of northern climate provided by the ocean. *Nat. Commun.*, **8**, 15875, https://doi.org/10.1038/ncomms15875.

——, R. C. J. Wills, H. L. Johnson, L. Chafik, and H. R. Langehaug, 2021: Mechanisms of decadal North Atlantic climate variability and implications for the recent cold anomaly. *J. Climate*, **34**, 3421–3439, https://doi.org/10.1175/JCLI-D-20-0464.1.

Athanasiadis, P. J., S. Yeager, Y.-O. Kwon, A. Bellucci, D. W. Smith, and S. Tibaldi, 2020: Decadal predictability of North Atlantic blocking and the NAO. *npj Climate Atmos. Sci.*, **3**, 20, https://doi.org/10.1038/s41612-020-0120-6.

——, and Coauthors, 2022: Mitigating climate biases in the midlatitude North Atlantic by increasing model resolution: SST gradients and their relation to blocking and the jet. *J. Climate*, **35**, 6985–7006, https://doi.org/10.1175/JCLI-D-21-0515.1.

Ba, J., and Coauthors, 2014: A multi-model comparison of Atlantic multidecadal variability. *Climate Dyn.*, **43**, 2333–2348, https://doi.org/10.1007/s00382-014-2056-1.

Baldwin, M. P., D. B. Stephenson, and I. T. Jolliffe, 2009: Spatial weighting and iterative projection methods for EOFs. *J. Climate*, **22**, 234–243, https://doi.org/10.1175/2008JCLI2147.1.

Barrier, N., C. Cassou, J. Deshayes, and A.-M. Treguier, 2014: Response of North Atlantic Ocean circulation to atmospheric weather regimes. *J. Phys. Oceanogr.*, **44**, 179–201, https://doi.org/10.1175/JPO-D-12-0217.1.

Bellomo, K., L. N. Murphy, M. A. Cane, A. C. Clement, and L. M. Polvani, 2018: Historical forcings as main drivers of the Atlantic multidecadal variability in the CESM large ensemble. *Climate Dyn.*, **50**, 3687–3698, https://doi.org/10.1007/s00382-017-3834-3.

Bellucci, A., S. Gualdi, E. Scoccimarro, and A. Navarra, 2008: NAO-ocean circulation interactions in a coupled general circulation model. *Climate Dyn.*, **31**, 759–777, https://doi.org/10.1007/s00382-008-0408-4.

——, and Coauthors, 2021: Air-sea interaction over the Gulf Stream in an ensemble of HighResMIP present climate simulations. *Climate Dyn.*, **56**, 2093–2111, https://doi.org/10.1007/s00382-020-05573-z.

Borchert, L. F., M. B. Menary, D. Swingedouw, G. Sgubin, L. Hermanson, and J. Mignot, 2021: Improved decadal predictions of North Atlantic Subpolar Gyre SST in CMIP6. *Geophys. Res. Lett.*, **48**, e2020GL091307, https://doi.org/10.1029/2020GL091307.

Bryan, F. O., M. W. Hecht, and R. D. Smith, 2007: Resolution convergence and sensitivity studies with North Atlantic circulation models. Part I: The western boundary current system. *Ocean Modell.*, **16**, 141–159, https://doi.org/10.1016/j.ocemod.2006.08.005.

Buckley, M. W., and J. Marshall, 2016: Observations, inferences, and mechanisms of the Atlantic meridional overturning circulation: A review. *Rev. Geophys.*, **54**, 5–63, https://doi.org/10.1002/2015RG000493.

Carmo-Costa, T., R. Bilbao, P. Ortega, A. Teles-Machado, and E. Dutra, 2022: Trends, variability and predictive skill of the ocean heat content in North Atlantic: An analysis with the EC-Earth3 model. *Climate Dyn.*, **58**, 1311–1328, https://doi.org/10.1007/s00382-021-05962-y.

Cayan, D. R., 1992: Latent and sensible heat flux anomalies over the northern oceans: The connection to monthly atmospheric circulation. *J. Climate*, **5**, 354–369, https://doi.org/10.1175/1520-0442(1992)005%3C0354:LASHFA%3E2.0.CO;2.

Chafik, L., N. P. Holliday, S. Bacon, and T. Rossby, 2022: Irminger Sea is the center of action for subpolar AMOC variability. *Geophys. Res. Lett.*, **49**, e2022GL099133, https://doi.org/10.1029/2022GL099133.

Chassignet, E. P., and Coauthors, 2020: Impact of horizontal resolution on global ocean-sea ice model simulations based on the experimental protocols of the Ocean Model Intercomparison Project Phase 2 (OMIP-2). *Geosci. Model Dev.*, **13**, 4595–4637, https://doi.org/10.5194/gmd-13-4595-2020.

Cherchi, A., and Coauthors, 2019: Global mean climate and main patterns of variability in the CMCC-CM2 coupled model. *J. Adv. Model. Earth Syst.*, **11**, 185–209, https://doi.org/10.1029/2018MS001369.

Cheung, A. H., M. E. Mann, B. A. Steinman, L. M. Frankcombe, M. H. England, and S. K. Miller, 2017: Comparison of low-frequency internal climate variability in CMIP5 models and observations. *J. Climate*, **30**, 4763–4776, https://doi.org/10.1175/JCLI-D-16-0712.1.

Curry, R. G., and M. S. McCartney, 2001: Ocean gyre circulation changes associated with the North Atlantic Oscillation. *J. Phys. Oceanogr.*, **31**, 3374–3400, https://doi.org/10.1175/1520-0485(2001)031%3C3374:OGCCAW%3E2.0.CO;2.

Czaja, A., and C. Frankignoul, 2002: Observed impact of Atlantic SST anomalies on the North Atlantic Oscillation. *J. Climate*, **15**, 606–623, https://doi.org/10.1175/1520-0442(2002)015%3C0606:OIOASA%3E2.0.CO;2.

——, A. W. Robertson, and T. Huck, 2003: The role of Atlantic Ocean–atmosphere coupling in affecting North Atlantic Oscillation variability. *The North Atlantic Oscillation: Climatic Significance and Environmental Impact*, *Geophys. Monogr.*, Vol. 134, Amer. Geophys. Union, 147–172, https://doi.org/10.1029/134GM07.

Danabasoglu, G., 2008: On multidecadal variability of the Atlantic meridional overturning circulation in the Community Climate System Model version 3. *J. Climate*, **21**, 5524–5544, https://doi.org/10.1175/2008JCLI2019.1.

——, and Coauthors, 2013: North Atlantic simulations in Coordinated Ocean-ice Reference Experiments phase II (CORE-

Brought to you by UNIV BOLOGNA-CAMPUS RAVENNA | Unauthenticated | Downloaded 02/14/24 03:05 PM UTC

II). Part I: Mean states. *Ocean Modell.*, **73**, 76–107, https://doi.org/10.1016/j.ocemod.2013.10.005.

——, and Coauthors, 2016: North Atlantic simulations in Coordinated Ocean-ice Reference Experiments phase II (CORE-II). Part II: Inter-annual to decadal variability. *Ocean Modell.*, **97**, 65–90, https://doi.org/10.1016/j.ocemod.2015.11.007.

de Coëtlogon, G., C. Frankignoul, M. Bentsen, C. Delon, H. Haak, S. Masina, and A. Pardaens, 2006: Gulf Stream variability in five oceanic general circulation models. *J. Phys. Oceanogr.*, **36**, 2119–2135, https://doi.org/10.1175/JPO2963.1.

Delworth, T. L., and F. Zeng, 2012: Multicentennial variability of the Atlantic meridional overturning circulation and its climatic influence in a 4000 year simulation of the GFDL CM2.1 climate model. *Geophys. Res. Lett.*, **39**, L13702, https://doi.org/10.1029/2012GL052107.

——, S. Manabe, and R. J. Stouffer, 1993: Interdecadal variations of the thermohaline circulation in a coupled ocean–atmosphere model. *J. Climate*, **6**, 1993–2011, https://doi.org/10.1175/1520-0442(1993)006%3C1993:IVOTTC%3E2.0.CO;2.

——, F. Zeng, L. Zhang, R. Zhang, G. A. Vecchia, and X. Yang, 2017: The central role of ocean dynamics in connecting the North Atlantic Oscillation to the extratropical component of the Atlantic multidecadal oscillation. *J. Climate*, **30**, 3789–3805, https://doi.org/10.1175/JCLI-D-16-0358.1.

Deser, C., and A. S. Phillips, 2021: Defining the internal component of Atlantic multidecadal variability in a changing climate. *Geophys. Res. Lett.*, **48**, e2021GL095023, https://doi.org/10.1029/2021GL095023.

——, ——, and M. A. Alexander, 2010: Twentieth century tropical sea surface temperature trends revisited. *Geophys. Res. Lett.*, **37**, L10701, https://doi.org/10.1029/2010GL043321.

Docquier, D., and Coauthors, 2019: Impact of model resolution on Arctic sea ice and North Atlantic Ocean heat transport. *Climate Dyn.*, **53**, 4989–5017, https://doi.org/10.1007/s00382-019-04840-y.

Dong, S., and K. A. Kelly, 2004: Heat budget in the Gulf Stream region: The importance of heat storage and advection. *J. Phys. Oceanogr.*, **34**, 1214–1231, https://doi.org/10.1175/1520-0485(2004)034%3C1214:HBITGS%3E2.0.CO;2.

Drews, A., and R. J. Greatbatch, 2016: Atlantic Multidecadal Variability in a model with an improved North Atlantic Current. *Geophys. Res. Lett.*, **43**, 8199–8206, https://doi.org/10.1002/2016GL069815.

Eden, C., and J. Willebrand, 2001: Mechanism of interannual to decadal variability of the North Atlantic circulation. *J. Climate*, **14**, 2266–2280, https://doi.org/10.1175/1520-0442(2001)014<2266:MOITDV>2.0.CO;2.

Fabiano, F., H. M. Christensen, K. Strommen, P. Athanasiadis, A. Baker, R. Schiemann, and S. Corti, 2020: Euro-Atlantic weather regimes in the PRIMAVERA coupled climate simulations: Impact of resolution and mean state biases on model performance. *Climate Dyn.*, **54**, 5031–5048, https://doi.org/10.1007/s00382-020-05271-w.

Famooss Paolini, L., P. J. Athanasiadis, P. Ruggieri, and A. Bellucci, 2022: The atmospheric response to meridional shifts of the Gulf Stream SST front and its dependence on model resolution. *J. Climate*, **35**, 6007–6030, https://doi.org/10.1175/JCLI-D-21-0530.1.

——, N.-E. Omrani, A. Bellucci, P. J. Athanasiadis, P. Ruggieri, C. R. Patrizio, and N. Keenlisyde, 2023: Non-stationarity in the NAO–Gulf Stream SST front interaction. *J. Climate*, submitted.

Ferreira, D., and C. Frankignoul, 2005: The transient atmospheric response to midlatitude SST anomalies. *J. Climate*, **18**, 1049–1067, https://doi.org/10.1175/JCLI-3313.1.

Frankignoul, C., and K. Hasselmann, 1977: Stochastic climate models, Part II Application to sea-surface temperature anomalies and thermocline variability. *Tellus*, **29A**, 289–305, https://doi.org/10.3402/tellusa.v29i4.11362.

——, G. de Coëtlogon, T. M. Joyce, and S. Dong, 2001: Gulf Stream variability and ocean–atmosphere interactions. *J. Phys. Oceanogr.*, **31**, 3516–3529, https://doi.org/10.1175/1520-0485(2002)031%3C3516:GSVAOA%3E2.0.CO;2.

——, E. Kestenare, and J. Mignot, 2002: The surface heat flux feedback. Part II: Direct and indirect estimates in the ECHAM$_4$/OPA8 coupled GCM. *Climate Dyn.*, **19**, 649–655, https://doi.org/10.1007/s00382-002-0253-9.

——, J. Deshayes, and R. Curry, 2009: The role of salinity in the decadal variability of the North Atlantic meridional overturning circulation. *Climate Dyn.*, **33**, 777–793, https://doi.org/10.1007/s00382-008-0523-2.

——, G. Gastineau, and Y.-O. Kwon, 2017: Estimation of the SST response to anthropogenic and external forcing and its impact on the Atlantic multidecadal oscillation and the Pacific decadal oscillation. *J. Climate*, **30**, 9871–9895, https://doi.org/10.1175/JCLI-D-17-0009.1.

Gastineau, G., and C. Frankignoul, 2015: Influence of the North Atlantic SST variability on the atmospheric circulation during the twentieth century. *J. Climate*, **28**, 1396–1416, https://doi.org/10.1175/JCLI-D-14-00424.1.

Good, S. A., M. J. Martin, and N. A. Rayner, 2013: EN4: Quality controlled ocean temperature and salinity profiles and monthly objective analyses with uncertainty estimates. *J. Geophys. Res. Oceans*, **118**, 6704–6716, https://doi.org/10.1002/2013JC009067.

Grist, J. P., S. A. Josey, A. L. New, M. Roberts, T. Koenigk, and D. Iovino, 2018: Increasing Atlantic ocean heat transport in the latest generation coupled ocean-atmosphere models: The role of air-sea interaction. *J. Geophys. Res. Oceans*, **123**, 8624–8637, https://doi.org/10.1029/2018JC014387.

Gutjahr, O., D. Putrasahan, K. Lohmann, J. H. Jungclaus, J.-S. von Storch, N. Brüggemann, H. Haak, and A. Stössel, 2019: Max Planck Institute Earth System Model (MPI-ESM1.2) for the High-Resolution Model Intercomparison Project (HighResMIP). *Geosci. Model Dev.*, **12**, 3241–3281, https://doi.org/10.5194/gmd-12-3241-2019.

Haarsma, R. J., and Coauthors, 2016: High Resolution Model Intercomparison Project (HighResMIP v1.0) for CMIP6. *Geosci. Model Dev.*, **9**, 4185–4208, https://doi.org/10.5194/gmd-9-4185-2016.

——, and Coauthors, 2020: HighResMIP versions of EC-Earth: EC-Earth3P and EC-Earth3P-HR—Description, model computational performance and basic validation. *Geosci. Model Dev.*, **13**, 3507–3527, https://doi.org/10.5194/gmd-13-3507-2020.

Häkkinen, S., P. B. Rhines, and D. L. Worthen, 2011: Atmospheric blocking and Atlantic multidecadal ocean variability. *Science*, **334**, 655–659, https://doi.org/10.1126/science.1205683.

Hall, A., and S. Manabe, 1997: Can local linear stochastic theory explain sea surface temperature and salinity variability? *Climate Dyn.*, **13**, 167–180, https://doi.org/10.1007/s003820050158.

Hersbach, H., and Coauthors, 2020: The ERA5 global reanalysis. *Quart. J. Roy. Meteor. Soc.*, **146**, 1999–2049, https://doi.org/10.1002/qj.3803.

Hewitt, H. T., and Coauthors, 2016: The impact of resolving the Rossby radius at mid-latitudes in the ocean: Results from a high-resolution version of the Met Office GC2 coupled

Brought to you by UNIV BOLOGNA-CAMPUS RAVENNA | Unauthenticated | Downloaded 02/14/24 03:05 PM UTC

model. *Geosci. Model Dev.*, **9**, 3655–3670, https://doi.org/10.5194/gmd-9-3655-2016.

——, and Coauthors, 2020: Resolving and parameterising the ocean mesoscale in Earth System models. *Curr. Climate Change Rep.*, **6**, 137–152, https://doi.org/10.1007/s40641-020-00164-w.

Hirschi, J. J.-M., and Coauthors, 2020: The Atlantic meridional overturning circulation in high-resolution models. *J. Geophys. Res. Oceans*, **125**, e2019JC015522, https://doi.org/10.1029/2019JC015522.

Hurrell, J. W., 1995: Decadal trends in the North Atlantic Oscillation: Regional temperatures and precipitation. *Science*, **269**, 676–679, https://doi.org/10.1126/science.269.5224.676.

——, and Coauthors, 2020a: NCAR CESM1-CAM5-SE-HR model output prepared for CMIP6 HighResMIP. Earth System Grid Federation, accessed 1 May 2022, https://doi.org/10.22033/ESGF/CMIP6.14220.

Hurrell, J., and Coauthors, 2020b: NCAR CESM1-CAM5-SE-LR model output prepared for CMIP6 HighResMIP. Earth System Grid Federation, accessed 1 May 2022, https://doi.org/10.22033/ESGF/CMIP6.14262.

Jackson, L. C., and Coauthors, 2019: The mean state and variability of the North Atlantic circulation: A perspective from ocean reanalyses. *J. Geophys. Res. Oceans*, **124**, 9141–9170, https://doi.org/10.1029/2019JC015210.

——, and Coauthors, 2020: Impact of ocean resolution and mean state on the rate of AMOC weakening. *Climate Dyn.*, **55**, 1711–1732, https://doi.org/10.1007/s00382-020-05345-9.

——, A. Biastoch, M. W. Buckley, D. G. Desbruyères, E. F. Williams, B. Moat, and J. Robson, 2022: The evolution of the North Atlantic meridional overturning circulation since 1980. *Nat. Rev. Earth Environ.*, **3**, 241–254, https://doi.org/10.1038/s43017-022-00263-2.

Jiang, W., G. Gastineau, and F. Codron, 2021: Multicentennial variability driven by salinity exchanges between the Atlantic and the Arctic Ocean in a coupled climate model. *J. Adv. Model. Earth Syst.*, **13**, e2020MS002366, https://doi.org/10.1029/2020MS002366.

Johnson, H. L., P. Cessi, D. P. Marshall, F. Schloesser, and M. A. Spall, 2019: Recent contributions of theory to our understanding of the Atlantic meridional overturning circulation. *J. Geophys. Res. Oceans*, **124**, 5376–5399, https://doi.org/10.1029/2019JC015330.

Joyce, T. M., C. Deser, and M. A. Spall, 2000: The relation between decadal variability of subtropical mode water and the North Atlantic Oscillation. *J. Climate*, **13**, 2550–2569, https://doi.org/10.1175/1520-0442(2000)013%3C2550:TRBDVO%3E2.0.CO;2.

Karspeck, A. R., and Coauthors, 2017: Comparison of the Atlantic meridional overturning circulation between 1960 and 2007 in six ocean reanalysis products. *Climate Dyn.*, **49**, 957–982, https://doi.org/10.1007/s00382-015-2787-7.

Keeley, S. P. E., R. T. Sutton, and L. C. Shaffrey, 2012: The impact of North Atlantic sea surface temperature errors on the simulation of North Atlantic European region climate. *Quart. J. Roy. Meteor. Soc.*, **138**, 1774–1783, https://doi.org/10.1002/qj.1912.

Kim, W. M., S. Yeager, P. Chang, and G. Danabasoglu, 2018: Low-frequency North Atlantic climate variability in the Community Earth System Model large ensemble. *J. Climate*, **31**, 787–813, https://doi.org/10.1175/JCLI-D-17-0193.1.

Knight, J. R., C. K. Folland, and A. A. Scaife, 2006: Climate impacts of the Atlantic multidecadal oscillation. *Geophys. Res. Lett.*, **33**, L17706, https://doi.org/10.1029/2006GL026242.

Koenigk, T., and Coauthors, 2021: Deep mixed ocean volume in the Labrador Sea in HighResMIP models. *Climate Dyn.*, **57**, 1895–1918, https://doi.org/10.1007/s00382-021-05785-x.

Kwon, Y.-O., and C. Frankignoul, 2012: Stochastically-driven multidecadal variability of the Atlantic meridional overturning circulation in $CCSM_3$. *Climate Dyn.*, **38**, 859–876, https://doi.org/10.1007/s00382-011-1040-2.

——, and ——, 2014: Mechanisms of multidecadal Atlantic meridional overturning circulation variability diagnosed in depth versus density space. *J. Climate*, **27**, 9359–9376, https://doi.org/10.1175/JCLI-D-14-00228.1.

——, H. Seo, C. C. Ummenhofer, and T. M. Joyce, 2020: Impact of multidecadal variability in Atlantic SST on winter atmospheric blocking. *J. Climate*, **33**, 867–892, https://doi.org/10.1175/JCLI-D-19-0324.1.

Lai, W. K. M., J. I. Robson, L. J. Wilcox, and N. Dunstone, 2022: Mechanisms of internal Atlantic multidecadal variability in HadGEM3-GC3.1 at two different resolutions. *J. Climate*, **35**, 1365–1383, https://doi.org/10.1175/JCLI-D-21-0281.1.

Larson, S. M., M. W. Buckley, and A. C. Clement, 2020: Extracting the buoyancy-driven Atlantic meridional overturning circulation. *J. Climate*, **33**, 4697–4714, https://doi.org/10.1175/JCLI-D-19-0590.1.

Lau, N.-C., and M. J. Nath, 2001: Impact of ENSO on SST Variability in the North Pacific and North Atlantic: Seasonal dependence and role of extratropical sea–air coupling. *J. Climate*, **14**, 2846–2866, https://doi.org/10.1175/1520-0442(2001)014%3C2846:IOEOSV%3E2.0.CO;2.

Lee, R. W., T. J. Woollings, B. J. Hoskins, K. D. Williams, C. H. O'Reilly, and G. Masato, 2018: Impact of Gulf Stream SST biases on the global atmospheric circulation. *Climate Dyn.*, **51**, 3369–3387, https://doi.org/10.1007/s00382-018-4083-9.

Liu, F., J. Lu, Y.-O. Kwon, C. Frankignoul, and Y. Luo, 2022: Freshwater flux variability lengthens the period of the low-frequency AMOC variability. *Geophys. Res. Lett.*, **49**, e2022GL100136, https://doi.org/10.1029/2022GL100136.

Liu, W., and A. Fedorov, 2022: Interaction between Arctic sea ice and the Atlantic meridional overturning circulation in a warming climate. *Climate Dyn.*, **58**, 1811–1827, https://doi.org/10.1007/s00382-021-05993-5.

Lohmann, K., H. Drange, and M. Bentsen, 2009: A possible mechanism for the strong weakening of the North Atlantic subpolar gyre in the mid-1990s. *Geophys. Res. Lett.*, **36**, L15602, https://doi.org/10.1029/2009GL039166.

Lozier, M. S., and Coauthors, 2019: A sea change in our view of overturning in the subpolar North Atlantic. *Science*, **363**, 516–521, https://doi.org/10.1126/science.aau6592.

Marshall, J., and Coauthors, 2001a: North Atlantic climate variability: Phenomena, impacts and mechanisms. *Int. J. Climatol.*, **21**, 1863–1898, https://doi.org/10.1002/joc.693.

——, H. Johnson, and J. Goodmann, 2001b: A study of the interaction of the North Atlantic Oscillation with ocean circulation. *J. Climate*, **14**, 1399–1421, https://doi.org/10.1175/1520-0442(2001)014%3C1399:ASOTIO%3E2.0.CO;2.

Martin, T., A. Reintges, and M. Latif, 2019: Coupled North Atlantic subdecadal variability in CMIP5 models. *J. Geophys. Res. Oceans*, **124**, 2404–2417, https://doi.org/10.1029/2018JC014539.

Marzocchi, A., J. J.-M. Hirschi, N. P. Holliday, S. A. Cunningham, A. T. Blaker, and A. C. Coward, 2015: The North Atlantic subpolar circulation in an eddy-resolving global ocean model. *J. Mar. Syst.*, **142**, 126–143, https://doi.org/10.1016/j.jmarsys.2014.10.007.

Brought to you by UNIV BOLOGNA-CAMPUS RAVENNA | Unauthenticated | Downloaded 02/14/24 03:05 PM UTC

Meccia, V. L., D. Iovino, and A. Bellucci, 2021: North Atlantic gyre circulation in PRIMAVERA models. *Climate Dyn.*, **56**, 4075–4090, https://doi.org/10.1007/s00382-021-05686-z.

——, R. Fuentes-Franco, P. Davini, K. Bellomo, F. Fabiano, S. Yang, and J. von Hardenberg, 2023: Internal multi-centennial variability of the Atlantic meridional overturning circulation simulated by EC-Earth3. *Climate Dyn.*, **60**, 3695–3712, https://doi.org/10.1007/s00382-022-06534-4.

Meehl, G. A., and Coauthors, 2019: Effects of model resolution, physics, and coupling on Southern Hemisphere storm tracks in CESM1.3. *Geophys. Res. Lett.*, **46**, 12 408–12 416, https://doi.org/10.1029/2019GL084057.

Megann, A., A. Blaker, S. Josey, A. New, and B. Sinha, 2021: Mechanisms for late 20th and early 21st century decadal AMOC variability. *J. Geophys. Res. Oceans*, **126**, e2021JC017865, https://doi.org/10.1029/2021JC017865.

Menary, M. B., and L. Hermanson, 2018: Limits on determining the skill of North Atlantic Ocean decadal predictions. *Nat. Commun.*, **9**, 1694, https://doi.org/10.1038/s41467-018-04043-9.

——, D. L. R. Hodson, J. I. Robson, R. T. Sutton, R. A. Wood, and J. A. Hunt, 2015a: Exploring the impact of CMIP5 model biases on the simulation of North Atlantic decadal variability. *Geophys. Res. Lett.*, **42**, 5926–5934, https://doi.org/10.1002/2015GL064360.

——, ——, ——, ——, and ——, 2015b: A mechanism of internal decadal Atlantic Ocean variability in a high-resolution coupled climate model. *J. Climate*, **28**, 7764–7785, https://doi.org/10.1175/JCLI-D-15-0106.1.

——, L. Hermanson, and N. J. Dunstone, 2016: The impact of Labrador Sea temperature and salinity variability on density and the subpolar AMOC in a decadal prediction system. *Geophys. Res. Lett.*, **43**, 12 217–12 227, https://doi.org/10.1002/2016GL070906.

——, and Coauthors, 2018: Preindustrial control simulations with HadGEM3-GC3.1 for CMIP6. *J. Adv. Model. Earth Syst.*, **10**, 3049–3075, https://doi.org/10.1029/2018MS001495.

——, L. C. Jackson, and M. S. Lozier, 2020: Reconciling the relationship between the AMOC and Labrador Sea in OSNAP observations and climate models. *Geophys. Res. Lett.*, **47**, e2020GL089793, https://doi.org/10.1029/2020GL089793.

Muir, L. C., and A. V. Fedorov, 2015: How the AMOC affects ocean temperatures on decadal to centennial timescales: The North Atlantic versus an interhemispheric seesaw. *Climate Dyn.*, **45**, 151–160, https://doi.org/10.1007/s00382-014-2443-7.

Murphy, L. N., K. Bellomo, M. Cane, and A. Clement, 2017: The role of historical forcings in simulating the observed Atlantic multidecadal oscillation. *Geophys. Res. Lett.*, **44**, 2472–2480, https://doi.org/10.1002/2016GL071337.

——, J. M. Klavans, A. C. Clement, and M. A. Cane, 2021: Investigating the roles of external forcing and ocean circulation on the Atlantic multidecadal SST variability in a large ensemble climate model hierarchy. *J. Climate*, **34**, 4835–4849, https://doi.org/10.1175/JCLI-D-20-0167.1.

North, G. R., T. L. Bell, R. F. Cahalan, and F. J. Moeng, 1982: Sampling errors in the estimation of empirical orthogonal functions. *Mon. Wea. Rev.*, **110**, 699–706, https://doi.org/10.1175/1520-0493(1982)110%3C0699:SEITEO%3E2.0.CO;2.

Oldenburg, D., R. C. J. Wills, K. C. Armour, L. Thompson, and L. C. Jackson, 2021: Mechanisms of low-frequency variability in North Atlantic Ocean heat transport and AMOC. *J. Climate*, **34**, 4733–4755, https://doi.org/10.1175/JCLI-D-20-0614.1.

——, ——, ——, and ——, 2022: Resolution dependence of atmosphere–ocean interactions and water mass transformation in the North Atlantic. *J. Geophys. Res. Oceans*, **127**, e2021JC018102, https://doi.org/10.1029/2021JC018102.

O'Reilly, C. H., D. J. Befort, A. Weisheimer, T. Woollings, A. Ballinger, and G. Hegerl, 2021: Projections of Northern Hemisphere extratropical climate underestimate internal variability and associated uncertainty. *Commun. Earth Environ.*, **2**, 194, https://doi.org/10.1038/s43247-021-00268-7.

Ortega, P., J. Robson, R. T. Sutton, and M. B. Andrews, 2017: Mechanisms of decadal variability in the Labrador Sea and the wider North Atlantic in a high-resolution climate model. *Climate Dyn.*, **49**, 2625–2647, https://doi.org/10.1007/s00382-016-3467-y.

——, and Coauthors, 2021: Labrador Sea subsurface density as a precursor of multidecadal variability in the North Atlantic: A multi-model study. *Earth Syst. Dyn.*, **12**, 419–438, https://doi.org/10.5194/esd-12-419-2021.

Park, T., W. Park, and M. Latif, 2016: Correcting North Atlantic sea surface salinity biases in the Kiel climate model: Influences on ocean circulation and Atlantic multidecadal variability. *Climate Dyn.*, **47**, 2543–2560, https://doi.org/10.1007/s00382-016-2982-1.

Petit, T., M. S. Lozier, S. A. Josey, and S. A. Cunningham, 2020: Atlantic Deep Water formation occurs primarily in the Iceland Basin and Irminger Sea by local buoyancy forcing. *Geophys. Res. Lett.*, **47**, e2020GL091028, https://doi.org/10.1029/2020GL091028.

Piecuch, C. G., R. M. Ponte, C. M. Little, M. W. Buckley, and I. Fukumori, 2017: Mechanisms underlying recent decadal changes in subpolar North Atlantic Ocean heat content. *J. Geophys. Res. Oceans*, **122**, 7181–7197, https://doi.org/10.1002/2017JC012845.

Reintges, A., M. Latif, and W. Park, 2017: Sub-decadal North Atlantic Oscillation variability in observations and the Kiel climate model. *Climate Dyn.*, **48**, 3475–3487, https://doi.org/10.1007/s00382-016-3279-0.

Roberts, C. D., R. Senan, F. Molteni, S. Boussetta, M. Mayer, and S. P. E. Keeley, 2018: Climate model configurations of the ECMWF Integrated Forecasting System (ECMWF-IFS cycle 43r1) for HighResMIP. *Geosci. Model Dev.*, **11**, 3681–3712, https://doi.org/10.5194/gmd-11-3681-2018.

——, F. Vitart, and M. A. Balmaseda, 2021: Hemispheric impact of North Atlantic SSTs in subseasonal forecasts. *Geophys. Res. Lett.*, **48**, e2020GL0911446, https://doi.org/10.1029/2020GL091446.

Roberts, M. J., and Coauthors, 2019: Description of the resolution hierarchy of the global coupled HadGEM3-GC3.1 model as used in CMIP6 HighResMIP experiments. *Geosci. Model Dev.*, **12**, 4999–5028, https://doi.org/10.5194/gmd-12-4999-2019.

——, and Coauthors, 2020: Sensitivity of the Atlantic meridional overturning circulation to model resolution in CMIP6 HighResMIP simulations and implications for future changes. *J. Adv. Model. Earth Syst.*, **12**, e2019MS002014, https://doi.org/10.1029/2019MS002014.

Robson, J., and Coauthors, 2018: Recent multivariate changes in the North Atlantic climate system, with a focus on 2005–2016. *Int. J. Climatol.*, **38**, 5050–5076, https://doi.org/10.1002/joc.5815.

Ruggieri, P., and Coauthors, 2021: Atlantic multidecadal variability and North Atlantic jet: A multimodel view from the Decadal Climate Prediction Project. *J. Climate*, **34**, 347–360, https://doi.org/10.1175/JCLI-D-19-0981.1.

Scaife, A. A., and D. Smith, 2018: A signal-to-noise paradox in climate science. *npj Climate Atmos. Sci.*, **1**, 28, https://doi.org/10.1038/s41612-018-0038-4.

Brought to you by UNIV BOLOGNA-CAMPUS RAVENNA | Unauthenticated | Downloaded 02/14/24 03:05 PM UTC

——, and Coauthors, 2011: Improved Atlantic winter blocking in a climate model. *Geophys. Res. Lett.*, **38**, L23703, https://doi.org/10.1029/2011GL049573.

——, and Coauthors, 2014: Skillful long-range prediction of European and North American winters. *Geophys. Res. Lett.*, **41**, 2514–2519, https://doi.org/10.1002/2014GL059637.

Schiemann, R., and Coauthors, 2020: Northern Hemisphere blocking simulation in current climate models: Evaluating progress from the Climate Model Intercomparison Project phase 5 to 6 and sensitivity to resolution. *Wea. Climate Dyn.*, **1**, 277–292, https://doi.org/10.5194/wcd-1-277-2020.

Sein, D. V., and Coauthors, 2017: Ocean modeling on a mesh with resolution following the local Rossby radius. *J. Adv. Model. Earth Syst.*, **9**, 2601–2614, https://doi.org/10.1002/2017MS001099.

Simpson, I. R., C. Deser, K. A. McKinnon, and E. A. Barnes, 2018: Modeled and observed multidecadal variability in the North Atlantic jet stream and its connection to sea surface temperatures. *J. Climate*, **31**, 8313–8338, https://doi.org/10.1175/JCLI-D-18-0168.1.

——, S. G. Yeager, K. A. McKinnon, and C. Deser, 2019: Decadal predictability of late winter precipitation in western Europe through an ocean–jet stream connection. *Nat. Geosci.*, **12**, 613–619, https://doi.org/10.1038/s41561-019-0391-x.

Siqueira, L., and B. P. Kirtman, 2016: Atlantic near-term climate variability and the role of a resolved Gulf Stream. *Geophys. Res. Lett.*, **43**, 3964–3972, https://doi.org/10.1002/2016GL068694.

Small, R. J., F. O. Bryan, S. P. Bishop, and R. A. Tomas, 2019: Air–sea turbulent heat fluxes in climate models and observational analyses: What drives their variability? *J. Climate*, **32**, 2397–2421, https://doi.org/10.1175/JCLI-D-18-0576.1.

Smith, D. M., and Coauthors, 2019: Robust skill of decadal climate predictions. *npj Climate Atmos. Sci.*, **2**, 13, https://doi.org/10.1038/s41612-019-0071-y.

——, and Coauthors, 2020: North Atlantic climate far more predictable than models imply. *Nature*, **583**, 796–800, https://doi.org/10.1038/s41586-020-2525-0.

Sun, C., J. Li, and F.-F. Jin, 2015: A delayed oscillator model for the quasi-periodic multidecadal variability of the NAO. *Climate Dyn.*, **45**, 2083–2099, https://doi.org/10.1007/s00382-014-2459-z.

Tsartsali, E. E., and Coauthors, 2022: Impact of resolution on the atmosphere–ocean coupling along the Gulf Stream in global high resolution models. *Climate Dyn.*, **58**, 3317–3333, https://doi.org/10.1007/s00382-021-06098-9.

Visbeck, M., E. P. Chassignet, R. G. Curry, T. L. Delworth, R. R. Dickson, and G. Krahmann, 2003: The ocean's response to North Atlantic Oscillation variability. *The North Atlantic Oscillation: Climatic Significance and Environmental Impact*, *Geophys. Monogr.*, Vol. 134, Amer. Geophys. Union, 113–145, https://doi.org/10.1029/134GM06.

Voldoire, A., and Coauthors, 2019: Evaluation of CMIP6 DECK experiments with CNRM-CM6-1. *J. Adv. Model. Earth Syst.*, **11**, 2177–2213, https://doi.org/10.1029/2019MS001683.

Wang, C., L. Zhang, S.-K. Lee, L. Wu, and C. R. Mechoso, 2014: A global perspective on CMIP5 climate model biases. *Nat. Climate Change*, **4**, 201–205, https://doi.org/10.1038/nclimate2118.

Wei, X., and R. Zhang, 2022: A simple conceptual model for the self-sustained multidecadal AMOC variability. *Geophys. Res. Lett.*, **49**, e2022GL099800, https://doi.org/10.1029/2022GL099800.

Wills, R. C. J., K. C. Armour, D. S. Battisti, and D. L. Hartmann, 2019: Ocean–atmosphere dynamical coupling fundamental to the Atlantic multidecadal oscillation. *J. Climate*, **32**, 251–272, https://doi.org/10.1175/JCLI-D-18-0269.1.

Wills, S. M., D. W. J. Thompson, and L. M. Ciasto, 2016: On the observed relationships between variability in Gulf Stream sea surface temperatures and the atmospheric circulation over the North Atlantic. *J. Climate*, **29**, 3719–3730, https://doi.org/10.1175/JCLI-D-15-0820.1.

Yan, X., R. Zhang, and T. R. Knutson, 2018: Underestimated AMOC variability and implications for AMV and predictability in CMIP models. *Geophys. Res. Lett.*, **45**, 4319–4328, https://doi.org/10.1029/2018GL077378.

Yeager, S., 2015: Topographic coupling of the Atlantic overturning and gyre circulations. *J. Phys. Oceanogr.*, **45**, 1258–1284, https://doi.org/10.1175/JPO-D-14-0100.1.

——, and G. Danabasoglu, 2014: The origins of late-twentieth-century variations in the large-scale North Atlantic circulation. *J. Climate*, **27**, 3222–3247, https://doi.org/10.1175/JCLI-D-13-00125.1.

——, and J. I. Robson, 2017: Recent progress in understanding and predicting Atlantic decadal climate variability. *Curr. Climate Change Rep.*, **3**, 112–127, https://doi.org/10.1007/s40641-017-0064-z.

——, and Coauthors, 2021: An outsized role for the Labrador Sea in the multi-decadal variability of the Atlantic overturning circulation. *Sci. Adv.*, **7**, eabh3592, https://doi.org/10.1126/sciadv.abh3592.

Zhang, R., 2008: Coherent surface-subsurface fingerprint of the Atlantic meridional overturning circulation. *Geophys. Res. Lett.*, **35**, L20705, https://doi.org/10.1029/2008GL035463.

——, and T. L. Delworth, 2006: Impact of Atlantic multidecadal oscillations on India/Sahel rainfall and Atlantic hurricanes. *Geophys. Res. Lett.*, **33**, L17712, https://doi.org/10.1029/2006GL026267.

——, R. Sutton, G. Danabasoglu, Y.-O. Kwon, R. Marsh, S. G. Yeager, D. E. Amrhein, and C. M. Little, 2019: A review of the role of the Atlantic meridional overturning circulation in Atlantic multidecadal variability and associated climate impacts. *Rev. Geophys.*, **57**, 316–375, https://doi.org/10.1029/2019RG000644.

Zhang, T., X. Shao, and S. Li, 2017: Impacts of atmospheric processes on ENSO asymmetry: A comparison between CESM1 and CCSM4. *J. Climate*, **30**, 9743–9762, https://doi.org/10.1175/JCLI-D-17-0360.1.

Brought to you by UNIV BOLOGNA-CAMPUS RAVENNA | Unauthenticated | Downloaded 02/14/24 03:05 PM UTC